Capicua regulates neural stem cell proliferation and lineage specification through control of Ets factors

Sheikh Tanveer Ahmad[1,2,3], Alexandra D. Rogers[2], Myra J. Chen[2,3], Rajiv Dixit[2,3,4], Lata Adnani[3,4], Luke S. Frankiw[2,5], Samuel O. Lawn[2,6], Michael D. Blough[2], Mana Alshehri[2,7], Wei Wu[2,8], Stephen M. Robbins[2], J. Gregory Cairncross[2], Carol Schuurmans[3,4], Jennifer A. Chan[1,2,3,*]

[1] Department of Pathology & Laboratory Medicine, University of Calgary, Calgary, Alberta, Canada
[2] Charbonneau Cancer Institute, University of Calgary, Calgary, Alberta, Canada
[3] Alberta Children's Hospital Research Institute, University of Calgary, Calgary, Alberta, Canada
[4] Sunnybrook Research Institute and the Department of Biochemistry, University of Toronto, Toronto, Ontario, Canada

Present addresses:
[5] Department of Biology & Bioengineering, California Institute of Technology, Pasadena, CA, USA
[6] Zymeworks, Vancouver, BC, Canada
[7] King Abdullah International Medical Centre, Riyadh, Saudi Arabia
[8] University of California, San Francisco, CA, USA

*Corresponding author:
Jennifer A. Chan
University of Calgary
Health Research and Innovation Centre, room 2A-A22
3330 Hospital Drive NW
Calgary, AB T2N 4N1
Canada
jawchan@ucalgary.ca

Keywords:
Capicua, CIC, oligodendroglioma, glioma, oligodendrocyte precursor cell, cell fate specification, gliogenesis, Etv5

ABSTRACT

Capicua (Cic) is a transcriptional repressor mutated in the brain cancer oligodendroglioma. Despite its cancer link, little is known of Cic's function in the brain. Here, we investigated the relationship between Cic expression and cell type specification in the brain. Cic is strongly expressed in astrocytic and neuronal lineage cells but is more weakly expressed in stem cells and oligodendroglial lineage cells. Using a new conditional *Cic* knockout mouse, we show that forebrain-specific *Cic* deletion increases proliferation and self-renewal of neural stem cells. Furthermore, *Cic* loss biases neural stem cells toward glial lineage selection, expanding the pool of oligodendrocyte precursor cells (OPCs). These proliferation and lineage selection effects in the developing brain are dependent on de-repression of Ets transcription factors. In patient-derived oligodendroglioma cells, CIC re-expression or ETV5 blockade decreases lineage bias, proliferation, self-renewal and tumorigenicity. Our results identify Cic is an important regulator of cell fate in neurodevelopment and oligodendroglioma, and suggest that its loss contributes to oligodendroglioma by promoting proliferation and an OPC-like identity via Ets overactivity.

INTRODUCTION

The identification of genes recurrently mutated in cancer often presents opportunities to uncover previously unappreciated mechanisms regulating normal development, and vice versa. The transcriptional repressor Capicua (*CIC*) has been identified as a likely tumour suppressor gene, as recurrent mutations in *CIC* and/or reduced expression of CIC are found in several cancer types. In the brain, *CIC* mutations are nearly exclusively found in oligodendrogliomas (ODGs) – glial tumors that are composed of cells resembling oligodendrocyte precursor cells (1, 2). Indeed, concurrent *IDH1/2* mutation, single-copy whole-arm losses of 1p and 19q, and mutation of the remaining copy of *CIC* on

58 chr 19q13 are highly characteristic of ODG and are not found in other cancer types (3-5). These
59 associations suggest a unique relationship between CIC and glial biology.
60
61 Prior work in Drosophila and in mammalian cultured cells has shown that Cic is a transcriptional
62 repressor downstream of receptor tyrosine kinase (RTK) signalling (6). Binding of Cic to the sequence
63 T(G/C)AATG(G/A)A in enhancers and promoters leads to transcriptional repression of its target genes
64 (7, 8). This default repression is relieved upon RTK signalling (6, 9-11), permitting transcription of targets
65 – among which are *PEA3/ETS* transcription factors *ETV1/4/5* (12). To date, there is limited knowledge
66 of Cic's function in mammalian development or in the brain. Recently, Yang et al. using *Cic* conditional
67 knockout mice, reported that Cic loss increases a population of proliferating Olig2+ cells in the brain,
68 and that) loss of Cic potentiates glial tumorigenesis in a glioma model driven by *PDGFR* (13). The
69 mechanisms by which Cic loss caused those findings, however, remained undefined. Meanwhile, in the
70 non-neoplastic context, Lu et al. recently showed that impairing the interaction of the Cic with the protein
71 Ataxin 1 results in spectrum of neurobehavioral and neurocognitive phenotypes, as well as abnormal
72 maturation and maintenance of populations of cortical neurons (14) – indicating a role for Cic in neuronal
73 biology as well. Deciphering Cic's mechanisms of action as a neurodevelopmental regulator may shed
74 light on these varied phenotypes resulting from Cic loss or abnormal function.
75
76 Here, we examine the temporal and spatial pattern of Cic expression in the mammalian cerebral cortex
77 and white matter, and take a loss-of-function approach to determine its role in neuronal-glial identity
78 determination. Our results reveal an important role for Cic in regulating the proliferation and lineage
79 specification of neural stem cells during development – with loss favoring NSC proliferation and glial
80 production at the expense of neuronal production. Furthermore, we show that these effects are mediated
81 largely through Cic's regulation of Ets factors. The proliferative dysregulation is recapitulated in
82 oligodendroglioma cells, where CIC re-expression or blockade of Ets activity reduces tumorigenicity.
83 Our findings reveal an important role for CIC in development and oligodendroglioma, and suggest that
84 Etv5 may be a potential therapeutic target.

85

86 **RESULTS**

87

88 **Nuclear Cic levels are cell type- and stage-specific**

89

90 As an initial step to investigating Cic's potential function in forebrain development and
91 oligodendroglioma, we examined its expression in several regions and cell types in the mouse brain.
92 Immunofluorescence staining for CIC and cell-type specific markers revealed that all cell types
93 examined have some detectable level of Cic protein, whether cytoplasmic or nuclear. Because of Cic's
94 previously identified role as a transcriptional repressor, however, we were particularly interested in the
95 nuclear levels and quantitated Cic nuclear staining intensity across cell types and stages.

96

97 Focusing first on the stem cell compartment, we assessed tissue from the dorsal telencephalon (the
98 anlage of the neocortex) at embryonic day (E) E12. At this early neurogenic stage, non-lineage restricted
99 neural stem cells (NSCs) are found in the ventricular zone (VZ) where can be identified by their spatial
100 location and their expression of the transcription factor Sox2 (15). In embryonic Sox2+ VZ cells, Cic was
101 localized predominantly in the cytoplasm, with relatively weak nuclear expression (Figure 1A). This
102 distribution is consistent with the previous demonstration that growth factor/RTK signaling is locally
103 elevated in the embryonic VZ (16, 17) and that Cic nuclear export is regulated by ERK-mediated Cic
104 phosphorylation (6, 9-11). Pools of stem/progenitor cells are not limited to development, but also persist
105 postnatally in the subventricular zone (SVZ) of the lateral ventricle and in the subgranular layer (SGL)
106 of the hippocampal dentate gyrus (18, 19). In the SVZ and SGL of postnatal day (P) P21 and P56 mice,
107 Cic was also weakly expressed within the nucleus in the Sox2+ compartment – in contrast to stronger
108 nuclear expression in adjacent differentiated cells (Figure 1B,C). Thus, in both the embryonic and
109 postnatal brain, neural stem cells are characterized by low levels of nuclear Cic.

110

111 As cells differentiated, Cic was increasingly localized to the nucleus, but with notable differences
112 between the levels detected in neuronal, astrocytic, and oligodendrocytic cell lineages. In the adult
113 (P56) cortex, NeuN+ neurons displayed the strongest nuclear Cic (Figure 1I). The increase in Cic within
114 the neuronal lineage was detectable during the process of embryonic neurogenesis, with a modest
115 increase detected as cells transitioned from Sox2+ stem cells to Tbr2+ neuronal intermediate
116 progenitors, followed by a more marked elevation in Tbr1+ post-mitotic neurons in the intermediate zone
117 and cortical plate – where nuclear Cic levels approached those of mature neurons in the adult cortex
118 (Figure 1G,H,I, J). In GFAP+ or Aldh1+ astrocytes in the cortex and underlying white matter, nuclear
119 Cic levels also increased relative to Sox2+ cells (Figure 1D,J; Supplemental Figure S1A). Among the
120 three major lineages, the lowest levels of nuclear Cic were found in the oligodendroglial lineage. Olig2
121 is a bHLH transcription factor that is expressed in cells at or before oligodendrocyte specification and
122 continues to be present throughout the stages of oligodendroglial differentiation (20, 21). Within the
123 Olig2+ population, the subset of Pdgfra+ cells indicative of oligodendrocyte precursor cells (OPCs) had
124 the lowest levels of all, with a modest increase in CNPase+ immature oligodendrocytes, and a further
125 increase in mature CC1+ oligodendrocytes (Figure 1E, F, J; and Supplemental Figure S1). Overall, the
126 mean integrated nuclear signal intensity for Cic was significantly lower in Sox2+ and Pdgfra+ cells than
127 in NeuN+ cells ($p < 0.0001$), Tbr1+ cells ($p < 0.0001$), or Gfap+ cells ($p < 0.01$) (Figure 1J and Suppl
128 S1).
129
130 As both NSCs and OPCs are cell types that are proliferation-competent, this pattern of lower nuclear
131 Cic in NSCs and OPCs, and higher nuclear Cic expression in neurons and astrocytes, raised the
132 possibility that nuclear CIC bound to its target genes may repress proliferation-related genes and/or
133 early oligodendroglial-promoting programs. We tested these hypotheses with a series of loss-of-function
134 studies.
135
136 **Cic-deficiency results in increased glial populations and decreased neuronal populations during**
137 **forebrain development**

138

139 Cic contains several critical domains including an HMG-box and a C-terminal C1 domain that together
140 bind to DNA, and a C-terminal Gro-L domain that mediates protein-protein interactions (10, 22-25). We
141 generated *Cic* conditional knockout mice in which exons 2-11 of *Cic* gene were flanked by loxP sites,
142 with the floxed region containing all exons encoding the HMG box. Upon introduction of Cre, exons 2-
143 11 are excised and the remaining exons 12-20 are frameshifted, thus ablating the HMG box, C1 domain,
144 and Gro-L domain (Figure 2A). We used these animals for in vivo studies as well as to generate cell
145 lines with which we could further study proliferation and lineage selection in a cell-autonomous manner.
146

147 By crossing *Cic*-floxed mice to *Foxg1-Cre* mice (in which *Cre* is expressed throughout the forebrain by
148 E10.5 (26)), we generated mice deficient in CIC in the embryonic telencephalon and subsequent
149 postnatal cerebrum (Figure 2A,B). $Cic^{Fl/Fl}$;$FoxG1^{Cre/+}$ animals were born in approximate Mendelian ratios
150 and were grossly indistinguishable at birth. They failed to thrive postnatally, however, becoming visible
151 runts by postnatal day 7, and were uniformly lethal by P22 when they did not survive past weaning
152 (Suppl Figure S2B). Gross and cursory light microscopic exam showed the presence of the expected
153 major anatomic structures in the brain, as well as the presence of laminated cortex, write matter tracts,
154 deep nuclei, and hippocampi (Suppl Figure S2A). The cerebra of Cic-null brains, however, were smaller
155 than littermate controls (Figure 2C). The reason for lethality is unclear. We have not found major
156 anatomic defects detected in other organs and suspect that poor feeding secondary to impaired
157 neurologic function may be related to their progressive decline. This, however, remains speculative.
158

159 Interestingly, closer evaluation of P21 cortices revealed a shift in cell populations, with decreased
160 neurons and increased oligodendroglia cells and astrocytes in Cic-null cortices compared to controls
161 (Fig 2D,D',E,E'). In Cic-null cortices, NeuN+ cells comprised 76.6±2.5% of total cells; whereas in
162 controls that were either CIC-floxed but without Cre ($Cic^{Fl/Fl}$; $FoxG1^{+/+}$) or that were heterozygous for Cic
163 loss ($Cic^{Fl/+}$; $FoxG1^{Cre/+}$), NeuN+ cells comprised 82.04±2.78% of the total cells (n=5, $p<0.05$). In
164 contrast, Gfap+ cells were increased in knockout relative to wild-type cortices (12.46±1.49 CIC-null *vs.*

165 9.61±1.39 Cic-wt; 1.29-fold change; n=5, p<0.05). Olig2+ cells were also increased in Cic-null cortices
166 compared to controls (10.83±1.47% *vs.* 4.99±0.87%, in Cic-null vs control, respectively; 2.17-fold
167 increased; n=5, p=0.0001), a finding corroborated by an increase in Sox10+ cells (11.72±1.83% *vs.*
168 7.43±0.94%; n=5, p=0.0001). In the progression along the oligodendrocyte lineage, the relative
169 distribution of cells was also altered. Olig2+Pdgfra+ OPCs were increased compared to controls
170 (44.53±3.80% of cells Olig2+Pdgfra+ in $CIC^{Fl/Fl}$;$FoxG1^{Cre/+}$ *vs.* 28.20±1.95% in controls; p<0.01),
171 whereas CNPase+ cells were comparatively decreased (*$CIC^{Fl/Fl}$;$FoxG1^{Cre/+}$* 38.0±9.78% *vs.* Control
172 72.92±3.88%; n=5, p<0.0001) (Figure 2E,E'). Mbp expression in the white matter was also decreased
173 in *$Cic^{Fl/Fl}$;$FoxG1^{Cre/+}$* brains (n=6, p < 0.01) (Figure 2E,E').
174
175 One possibility that could explain such a skewing of cell populations could be that there was increased
176 death in a particular population. However we found no evidence of increased apoptosis in the knockout
177 brains (Suppl Fig S3E). Other possibilities, were that Cic loss could be increasing proliferation and
178 affecting lineage selection in NSCs, or that Cic loss could have specific effects on OPC proliferation and
179 maturation – possibilities that are not mutually exclusive. In the following work, we focus our
180 investigations on Cic's role at the NSC stage, and examine its role in proliferation and lineage selection.
181
182 **CIC increases proliferation of neural stem cells**
183
184 Others recently reported proliferative gains upon loss of Cic (13), and we too found evidence of this. By
185 electroporating pCIG2-Cre (or pCIG2 empty vector control) into *$Cic^{Fl/Fl}$* embryos, we could study the
186 effects of Cic loss in a discrete population of VZ cells and their subsequent progeny (schematic Figure
187 4A). 48 hours after Cre electroporation into VZ NSCs at E13 (early to mid-neurogenesis), EdU
188 incorporation was markedly increased, as were the numbers of Sox2 positive cells. Among GFP+ cells,
189 EdU+ cells were increased by 2.6-fold in cre- vs. control-electroporated brains (pCIG2-Cre 9.99±0.92%
190 Edu+, n=4, *vs.* pCIG2-Empty; 3.77±0.81%, n=5, p<0.0001)(Figure 3A,A'). The fraction of GFP+ cells
191 expressing Sox2 was also increased (pCIG2-Cre 11.09±1.10% Sox2+ vs. pCIG2-Empty 5.48±1.01%;

192 n=4 and n=5, respectively; $p<0.05$) (Figure 4B,B'). There was no change in activated Caspase-3,
193 indicating that the increased Sox2+ fraction in Cic-deleted cells was due to increased apoptosis in other
194 cells (Suppl Figure S3D,D'). Together, these findings supported a cell-autonomous increase in NSC
195 proliferation with CIC loss. Of note, there was also an increase in Edu+ cells among non-GFP cells
196 within the area of the electroporated patches, suggesting additional non-cell autonomous effects which
197 we did not pursue.
198
199 To confirm the cell autonomous gains in NSC proliferation with CIC ablation, we turned to cell culture.
200 *Cic* null and control NSC lines were derived from E15 *Cic*-floxed cells transfected ex-vivo with Cre or
201 control plasmids (Figure 3B). When maintained in serum-free NSC proliferation media, Cic-null and
202 control cells both maintained expression of NSC markers such as the intermediate filament protein
203 nestin (Figure 5A,B). When Cic-null and control cells were seeded at equal numbers and grown in NSC
204 proliferation media, however, Cic-null cells displayed a 3-fold increase in cell numbers relative to controls
205 by 3 days post-plating (Cic-null; 2.90±0.44, n=4, *vs.* Cic-wt; 0.98±0.12, n=3, $p<0.01$) (Figure 3C). These
206 data were corroborated by Alamar blue cell viability assay (Suppl Figure S3A), Ki-67 immunostaining
207 (Figure 3D) and cell cycle analysis (Figure 3E), all of which showed increased proliferation in Cic-null
208 cultures compared to controls. There were no significant differences in the numbers of dead cells (Suppl
209 Figure S3C), supporting that the differences in viable cell numbers for Cic-null cells was due to their
210 higher proliferative rates, rather than reduced cell death. Together, the data show that Cic is a strong
211 negative regulator of proliferation in forebrain NSCs.
212
213 ***Cic* loss alters mode of cell division and self-renewal**
214
215 During mammalian neurodevelopment, the stem cell pool is first expanded by symmetric proliferative
216 cell divisions followed by rounds of asymmetric divisions of stem and progenitor cells, which generate
217 neurons and then glia, and finally by terminal symmetric differentiative divisions (18). The balance

218 between symmetric and asymmetric divisions is important for maintaining the stem/progenitor pool, and
219 alterations in cell division mode can lead to neoplasia (27).
220
221 To investigate whether *Cic* loss alters modes of cell division, we performed a paired cell assay. *Cic* null
222 and control NSCs were seeded at low density in adherent cultures for 24 hrs, then fixed and stained for
223 Ki-67 (Figure 3G). Pairs where both daughter cells were Ki67+ were scored as symmetric proliferative
224 divisions. Pairs where daughter cells differed in Ki67 expression (i.e. Ki67+/Ki67-) were scored as
225 asymmetric. Pairs where both daughter cells were Ki67- were scored as symmetric terminal. *Cic* null
226 cells, underwent significantly more frequent symmetric proliferative divisions (77.6 ± 10.2% vs. 24.3 ±
227 4.9%; $p < 0.01$, n=3) and fewer asymmetric divisions (9.7 ± 1.2% vs. 64.0 ± 7.1%; $p < 0.05$, n=3)
228 compared to controls (Figure 3H). No significant difference was found in numbers of symmetric terminal
229 divisions between *Cic* null and control cells, although there was a trend toward decreased terminal
230 divisions in CIC null cells (12.7 ± 8.1% vs. 25.0 ± 6.5%; n=3, $p = 0.108$)(Figure 3H). The net effect of
231 these is the presence of more cycling and self-renewing cells.
232
233 Consistent with this, evidence for increased self-renewal in the Cic null cells was also detected in a
234 clonogenic assay (Figure 3F). In this assay, after plating equal numbers of dissociated cells in semi-
235 solid media, a higher number of spheres indicates higher number of self-renewing cells in the initial
236 population, whereas sphere volume is a more general indicator of proliferation that includes the
237 influence of factors such as cell cycle kinetics, modes of cell division, and the fraction of cells remaining
238 in or exiting the cell cycle. Both Cic-null and control NSCs were able to generate spheres, but Cic-null
239 NSCs NSCs generated higher sphere counts (n=3; $p < 0.0001$) and larger spheres compared to control
240 (n=3; $p<0.0001$)(Figure 3F,F',F''). Thus, Cic loss confers not only higher proliferation but higher self-
241 renewal capacity in NSCs, at least when cells are in an environment promoting NSC proliferation.
242
243 ***Cic* ablation in NSCs increases the pool of cells expressing glial lineage determinants**
244

245 While the proliferative effects of Cic deficiency in NSCs were clear, what was intriguing was the
246 additional possibility that Cic loss may be affecting lineage selection in NSCs. The *Cic*$^{Fl/Fl}$*;FoxG1*$^{Cre/+}$
247 phenotype (Figure 2) was characterized by a shift in cell populations with fewer neurons and increased
248 glia (Figure 2). We thus asked whether Cic loss had altered the expression of factors important in
249 regulating lineage selection and gliogenic potential.
250
251 To this end, we examined the expression of Sox 9 and Olig2 in Cic-wildtype and -null NSCs. Sox9 is an
252 HMG-box transcription factor present in a range of CNS cell types, including stem cells, astrocyte and
253 oligodendroglial precursors, and later glial cells. It has key roles not only in stem cell maintenance but
254 also in driving differentiation programs away from neurogenesis and towards gliogenesis of both
255 astrocytes and oligodendrocytes at the stage of gliogenic initiation (28-30). Similarly, Olig2 is expressed
256 in a multitude of cells including stem cells, oligodendroglial lineage cells, and specific subtypes of
257 neurons; but it has a major role in establishing oligodendroglial competence. In our control or cre-
258 electroporated brains where Cre was introduced at E13, we found that the fraction of GFP+ cells
259 expressing Sox9 was 2.5-fold increased over controls at 2 days post-electroporation (pCIG2-Cre;
260 15.97±1.69% *vs.* pCIG2-Empty; 6.37±1.60%, n=4 $p<0.05$) (Figure 4C,C'). Following the targeted cells
261 to E18 (5 days post-electroporation) revealed that a smaller fraction Cic-deleted NSCs subsequently
262 became Tbr1+ early-born/deep-layer neurons (pCIG2-Cre 1.66±0.91% *vs.* pCIG2-Empty 4.62±1.04%;
263 n=5, $p<0.01$) (Figure 4D,D'). Conversely, a greater number fraction became Aldh1+ astrocytes (pCIG2-
264 Cre 3.65±1.31%, n=5, *vs.* p-CIG2-Empty 1.664±0.91%, n=6; $p<0.05$) or Pdgfra+ OPCs (pCIG2-Cre
265 13.29±1.04%, *vs.* p-CIG2-Empty 5.87±2.54%; n=4; $p<0.01$) (Figure 4C,C',E,E').
266
267 These findings were echoed in the expression of stem and lineage markers in the cultured NSCs. As
268 expected, when cells were grown in NSC media, both Cic-null and control cells both strongly expressed
269 Nestin, and were largely devoid of Gfap or the pan-neuronal marker βIII-Tubulin (as detected by
270 Tuj1)(Figure 5A,B), or markers of subsequent oligodendrocyte stages, including OPCs, mature, and
271 myelinating oligodendrocytes (not shown). There, was, however, a marked increase in the percentage

272 of cells expressing Sox9 and Olig2 in Cic-null cultures (Figure 5A,A'). Sox9+ cells were increased 3.04-
273 fold in Cic-null cultures compared to control (Cic-null 37.4±3.6% *vs.* Cic-wt 12.3±2.1%; n=3, p <
274 0.01)(Figure 5A,B) while Olig2+ cells were increased 2.09-fold (Cic-null 29.8±2.9% *vs.* Cic-wt 14.2±3.5%
275 in controls; n=3, p<0.01) (Figure 5A,A'). Western blotting also corroborated the findings (Figure 5B). A
276 possible interpretation of the increased Sox9 and Olig2 concurrent with Nestin positivity in Cic-null cells
277 is that Cic loss may set an intrinsic foundation for pro-glial or pro-oligodendroglial programs starting
278 early in the neural cellular hierarchy.
279
280 **Cic-deficient NSCs are less responsive to extrinsic neuronal and astrocytic lineage selection**
281 **cues, but are biased to oligodendroglial lineage selection**
282
283 To directly test cell type specification capacity, we challenged Cic-null and control NSCs with exposure
284 to different lineage-promoting culture conditions. Neuronal differentiation was induced by culturing cells
285 with B27 and cAMP. Astrocytic differentiation was induced by culturing NSCs in 1% FBS and N2.
286 Oligodendroglial differentiation was induced by culturing cells in media with B27 and tri-iodo-thyronine.
287 After a 10 day exposure to these conditions, cultures were analyzed for cellular identity and morphology.
288
289 After 10 days in the neuronal condition, fewer Tuj1+ cells were generated in absolute numbers in Cic
290 null cultures compared to controls after plating equal numbers of starting cells (1.967±0.36 $x10^3$ vs
291 2.929±0.33 $x10^3$ Tuj1+ per well in Cic-null vs control; p<0.05)(Fig 6G) – a finding corroborated by
292 western blotting for Tuj1 (Figure 5C'). Furthermore, of the cells that were Tuj1+, we observed fewer
293 and less complex cell processes in the Cic-null cells than in their Cic-wildtype counterparts (Figure 5C).
294 In the astrocytic condition, there were fewer absolute numbers of Gfap+ cells in the Cic-null cultures
295 (1.471±0.15 $x10^3$ vs 2.74±0.55 $x10^3$ Gfap+ per well in Cic-null vs control, p<0.05) (Fig 6F). Western
296 blotting also showed decreased GFAP (Figure 5D'). Analogous to our observation in the neuronal
297 differentiation condition, Gfap+ Cic-null cells in the astrocytic differentiation condition displayed more
298 rudimentary processes than their Cic-wildtype counterparts (Figure 5D). When viewed as fractions of

299 the total cell population, Cic-null cultures were comprised of a significantly smaller fraction of bIII-Tub+
300 (Tuj1+) neurons in the neuronal condition (CIC-null 24.0±9.2% *vs.* CIC-wt 67.8±8.5%, respectively; n=3,
301 p<0.01) and a significantly smaller fraction of Gfap+ cells in the astrocytic condition (29.1±5.5% in Cic-
302 null *vs.* 68.2±10.4% in Cic-wt; n=3, p <0.01)(Figure 5C,D). In both of these conditions, there were only
303 a few proliferating cells remaining after the differentiation protocols. In both conditions, there was also
304 no change in apoptotic cells (Suppl Figure S2F-F'''). Together, the data indicate that Cic-deficient NSCs
305 are less responsive to external cues for neuronal and astrocytic lineage specification.
306
307 We then asked what the Cic-null NSCs became, if not neurons and astrocytes, respectively. In the
308 neuronal condition, the Tuj1- population was predominantly comprised of Sox2+ cells, followed by
309 Olig2+ cells; together, half of the culture was comprised of either Sox2+ (31%) or Olig2+ cells (19%)
310 after exposure to the neuronal conditions (Figure 6B',B'''). Of the Sox2+ and Olig2+ cells present,
311 however, less than 1% were EdU+, and there was no significant difference between the proliferation
312 rate of Sox2+ or Olig2+ cells in the Cic-null vs. control cultures in the neuronal condition (Figure 6D-E).
313 There was also a small but non-significant increase in the percentage of Gfap+ cells in the Cic-null
314 cultures compared to control. In the astrocytic culture condition, the Gfap- population was also
315 comprised predominantly of Sox2+ cells and, to a lesser extent Olig2+ cells, both of which were
316 significantly increased in the Cic-null cultures compared to controls. 36% of the Cic-null cells in the
317 astrocytic condition still expressed Sox2 after the 10-day protocol (Figure 6A'''). Tuj1+ cells were rare
318 in the astrocytic condition in both Cic-null and control cultures. These data further support that CIC-
319 deficient NSCs are less responsive to neuronal and astrocytic lineage cues, and instead remain as stem
320 cells that are permissive to the oligodendroglial lineage.
321
322 After 10 days in the oligodendrocyte-promoting media both Cic-null and wildtype cultures contained a
323 mix neurons, astrocytes, and oligodendrocytes; however the distributions of cells between cell types
324 and also along stages of oligodendrocyte lineage progression were altered. There was a higher fraction
325 of Olig2+ cells in Cic-null cultures compared to control (Cic-null 68.0±1.6% *vs.* Cic-wt 54.1±0.9%; n=3,

326 $p < 0.01$) as well as increased Olig2 by western blotting (Figure 5E). When analyzed for markers of
327 OPCs versus more mature oligodendroglial markers, Cic-null cells also had a greater percentage of
328 Olig2+ Pdgfra+ cells than in Cic-wildtype cultures (Cic-null 68.8±2.4% vs. Cic-wt 39.3±3.8%; n=5, $p <$
329 0.0001)(Figure 5E). Conversely the percentage of Olig2+MBP+ cells was decreased in Cic-null cultures
330 compared to controls (Cic-null 2.1±1.5% vs. Cic-wt 8.2±3.0%; n=5, $p < 0.0001$)(Figure 5E). Of the few
331 Cic-null Olig2+MBP+ cells that were identified, process formation was rudimentary compared to Cic-
332 wildtype cells. With respect to other cell types present in the oligodendroglial culture conditions, Sox2+
333 cells were increased in Cic-null cultures compared to control, whereas both Tuj1+ and Gfap+ cells were
334 reduced (Figure 6C-C''').
335
336 The results suggest to us that Cic-null cells are less sensitive to neuronal or astrocytic differentiation
337 signals but retain permissiveness to the oligodendroglial lineage. Cumulatively, based on the pattern of
338 cell-type specific nuclear Cic expression in forebrain tissue together with the in vivo and in vitro functional
339 studies of Cic ablation, we conclude that Cic is a critical regulator of proliferation, self-renewal, and cell
340 fate of NSCs. Loss of Cic expands the OPC pool by not only increasing NSC proliferation but also
341 biasing their specification towards the oligodendroglial lineage.
342
343 **Ets factors are transcriptional repressive targets of Cic in the forebrain**
344
345 As Cic is a transcriptional repressor, one mechanism for our findings is that Cic loss de-represses
346 specific genes driving NSC proliferation and lineage specificaiton. In this respect, *Etv* genes, which
347 encode Ets-domain transcription factors, are candidate target genes of interest. *Etv* genes (Etv 1, 4, 5)
348 have been identified as direct targets of Cic in various mammalian cells and tissues (12, 31), and are
349 overexpressed in ODGs (32). Furthermore, previous studies have documented Cic occupancy at the
350 *Etv5* promoter, at least in cerebellar tissue (33). Consistent with a possible functional relationship
351 between CIC and Ets factor gene regulation in the forebrain, we found that NSCs and OPCs, the two
352 cell types that have the the lowest levels of nuclear Cic (Figure 1), express the highest levels of Etv4

353 and 5 (Figure 7F-K; Supplemental Figure S5B-D'). We also confirmed that in forebrain tissue, *Etv5*
354 showed evidence of promoter occupancy by Cic via ChIP-PCR (Figure 7C).
355
356 If Ets factors are the mediators of the effects of CIC loss that we observe, we would expect their levels
357 to be elevated in our experimental systems of CIC loss. Indeed, we found that *Etv4* and *Etv5* transcript
358 levels were elevated in cultured Cic-null cells compared to control cells after 2 days of growth in
359 oligodendroglial conditions. *Etv5* mRNA was increased ~37 fold while *Etv4* transcripts were increased
360 ~19 fold in Cic-null cells versus control cells whereas *Etv1* transcripts were unchanged (Figure 7A).
361 Western blotting also confirmed marked increases in levels of Etv4 and Etv5 in Cic-null cells (Figure
362 7B). Although both *Etv4* and *Etv5* were both de-repressed upon Cic loss, because of the comparatively
363 higher levels of Etv5 relative to Etv4, as well as previous studies implicating *Etv5* in mediating glial fate
364 decisions (34), we focused additional studies on this Ets factor. In vivo electroporation of *Cic* shRNA
365 into the telencephalic VZ resulted in upregulation of *Etv5* transcript in the electroporated patch within 48
366 hours (Figure 7D). Our *Cic*-floxed, Cre-electroporated brains showed a similar increase in Etv5 protein
367 in the electroporated patch (Figure 7E). In aggregate, these data support that the PEA3 Ets transcription
368 factors are transcriptional repressive targets of Cic in the forebrain.
369
370 **Ets de-repression mediates the proliferative and oligo-biased phenotype of *Cic*-deficient NSCs**
371
372 To determine whether the increased proliferation and OPC bias that we observed with CIC ablation was
373 mediated by Etv5, we overexpressed wild-type *Etv5*. In vivo, electroporation of wild-type *Etv5*
374 phenocopied the increase proliferation of CIC-null cells in vivo (Figure 8D, D', S5A). Similarly, *Etv5*
375 overexpression acutely increased proliferation of cultured NSCs (Figure 8F, S5C'). We also performed
376 epistasis experiments introducing a dominant negative form (*DNETV5*) in which *Etv5* was fused to the
377 *Engrailed* transcriptional repressor domain. Introduction of *DNETV5* or knockdown of *Etv5* with siRNA
378 reduced the proliferation of cultured *Cic*-deficient NSCs back to control levels (Figure 8F-G, Suppl Figure
379 S5). In vivo, the increased proliferation observed upon deletion of *Cic* by cre-electroporation was

380 abrogated by co-electroporation with *DNETV5,* resulting in proliferation that was comparable to baseline
381 (Figure 8E, E' compared to 8D,D'; Figure S5). Based on the extent of the effects of *Etv5* overexpression
382 and *DNETV5* rescue in these assays, we conclude that the proliferative effects of Cic loss are large
383 driven by derepression of Etv5.
384
385 With respect to the altered proportions of cell types that we had observed in CIC-deficient NSCs exposed
386 to the different lineage-specific culture conditions, overexpression of wild-type Etv5 also phenocopied
387 CIC loss in many respects. There were decreased fractions of Tuj1+ cells and Gfap+ cells in the
388 neuronal and astrocytic conditions, and increased fractions of Olig2+ and Olig2+Pdgfra+ cells in the
389 oligodendrocytic condition when Etv5 was overexpressed – although the severity of the changes was
390 somewhat less marked with Etv5 overexpression compared to Cic loss. DNETV5 was also able to
391 substantially (although incompletely) rescue the phenotype of Cic-deficient cells in these assays. In the
392 neuronal and astrocytic conditions, DNETV5 significantly increased the populations of Tuj1+ and Gfap+
393 cells, respectively. The shifts in Olig2+ cells and Olig2+Pdgfra+ OPCs returned to control levels
394 (44.6±12.0% in *Cic*^{null}*;DNETV5* cells *vs.* 62.5±14.6% in *Cic*^{null} cells; n=3, $p<0.05$). The percentage of cells
395 expressing MBP also showed a substantial although partial rescue (5.3±2.9% in *Cic*^{null}*;DNETV5* cells
396 *vs.* 2.1±1.5% in *Cic*^{null} cells; n=3, $p < 0.05$) (Figure 8C-C'). That the extent of the changes for the lineage
397 selection assays with Etv5 overexpression and DNETV5 rescue were partial suggests that other factors
398 may contribute to the lineage specification affects, nevertheless the results point to Etv5 as playing a
399 large part in the lineage phenotype.
400
401 Thus, Etv5 is both necessary and sufficient for inducing the proliferation and cell fate bias effects
402 downstream of CIC loss.
403
404 **Ets blockade decreases proliferation, self-renewal, and tumorigenicity of human**
405 **oligodendroglioma cells**
406

407 Finally, we used 2 oligodendroglioma cell lines, BT54 and BT88, to further investigate the importance
408 of *CIC* mutation/loss in human disease. Both of these patient-derived lines harbour the characteristic
409 whole-arm chromosome 1p and 19q losses that are diagnostic of ODG (35). As well, BT54 harbours a
410 splice acceptor site mutation in the remaining *CIC* exon 6 while BT88 harbours a missense mutation in
411 the remaining *CIC* exon 20 (3). In both BT54 and BT88, either stable re-expression of wildtype CIC or
412 stable expression of *DNETV5* significantly reduced proliferation as measured by EdU incorporation
413 (Figure 9A,A',C). Sphere-forming ability was also decreased by *CIC* expression or by introduction of
414 *DNETV5* (Figure 9B,B',B'',D,E). These results were also confirmed by transient siRNA experiments to
415 knock down Etv5 in BT-88 cells that also showed decreased proliferation and sphere formation (data
416 not shown). Consistent with an ongoing requirement for CIC loss or Etv5 expression for proliferation
417 and self-renewal in ODG, in vivo tumorigenicity of BT88 cells was markedly reduced by stable
418 expression of either wildtype *CIC* or *DNETV5* (Figure 10). Thus, in cells that are already transformed to
419 ODG, CIC loss and the subsequent elevation of Etv5 remains important to sustain the proliferative
420 phenotype.
421
422 A similar finding was observed when we assessed the ODG cell lines' ability to differentiate in response
423 to oligodendrocyte differentiation conditions. Both CIC re-expression and DNETV5 similarly resulted in
424 increased expression of CNPase in the ODG cells compared to BT-88 control cells, indicating at least
425 some improvement in capacity for the tumour cells to differentiate and mature (Figure 9F,F' bottom row
426 panels). Interestingly, however, effects on neuronal and astrocytic differentiation, were mixed (Figure
427 9F,F' top and middle row panels). Cic re-expression resulted increased the ability of cells to respond to
428 extrinsic neuronal differentiation cues by increasing expressing bIII-Tubulin (TUJ1) and extending
429 neurites; however this was not phenocopied by DNETV5. With respect to expression of GFAP in
430 response to astrocytic differentiation cues, no significant differences were detected with either CIC re-
431 expression or DNETV5 introduction compared to BT-88 control. The latter data suggest that other
432 genetic (or epigenetic) alterations may be more central to driving or maintaining some specific aspects
433 of the tumour cells' phenotypes, at least in our cultured system. The effects on differentiation in vivo

434 were not evaluated, however, as the lesions resulting from implantation of CIC- or DNETV5-expressing
435 BT88 cells were too small to provide meaningful cell numbers for assessment.
436
437 Taken together, our results indicate that Cic regulates NSC proliferation and cell fate in
438 neurodevelopment and oligodendroglioma, and that the pro-proliferative and pro-OPC phenotypes
439 observed with Cic loss are largely mediated through Ets transcriptional de-repression.
440
441 **DISCUSSION**
442
443 Genomic analyses of brain cancers have suggested that *CIC* functions as a tumor suppressor gene in
444 diffuse gliomas, particularly ODGs (3, 4, 36). Yet, to date, knowledge of *CIC*'s role in the brain has been
445 limited. Here we report previously undescribed cell type specific differences in CIC expression in the
446 brain. Moreover, our functional work examining *Cic* function in forebrain development and in
447 oligodendroglioma cells provides new insight into the roles of this putative tumor suppressor in
448 regulating the developmental fate of neural stem/progenitor cells.
449
450 We found that genetic ablation of Cic biases cells neural stem cells away from neuronal lineage
451 specification to the selection of glial lineages. Adding to knowledge that RAS/MAPK pathway signaling
452 regulates the switch from neurogenesis to gliogenesis, with *ETV5* implicated in mediating gliogenic
453 competence (17, 34), our results firmly place *Cic* at the intersection of RAS pathway signaling and *Etv5*
454 in the brain, providing a missing link between extrinsic differentiation signals and the execution of
455 transcriptional programs critical for normal neuro- and glio-genesis. With respect to Cic and the anti-
456 neuronal bias that we observed, recent work by Lu, et al. found that disrupting Ataxin-1 (Atxn1)-Cic
457 complexes resulted in abnormal maturation and maintenance of upper-layer cortical neurons – with
458 concomitant effect on behavior, learning, and memory (14). It is unknown, however, the extent to which
459 the effects could be due to specific Ataxin-Cic interactions versus Cic abnormality alone. Our studies,
460 which primarily focused on early lineage selection events, did not systematically address questions of

461 cell maturation (although some of our in vitro morphological findings are consistent with a neuronal
462 maturation defect). Future work would be needed to define the complex neuronal dependencies on Cic,
463 not only in the forebrain but also in the cerebellum where Cic pathology has also been implicated (37)
464 (38).
465
466 With respect to neural stem cell proliferation, glial fates, and the implications for ODG; our findings build
467 on the recent observation by Yang, et al. that CIC deficiency increases a population of proliferating
468 OPCs in the brain (13). Our work is not only consistent, but now provides a mechanistic foundation for
469 the observations with identification of symmetric cell divisin alterations, dissection of lineage selection
470 effects and identification of a downstream mediator. Together, they provide tangible links between *CIC*
471 loss and ODG biology – as both dysregulated proliferation and the persistence of an immature OPC
472 phenotype are cardinal features of this cancer. Many parallels exist between normal OPCs and the cells
473 comprising ODG. In common, both OPCs and ODGs express PDGF, PDGFR, and NG2, which control
474 OPC differentiation (39, 40). Together, the results may thus explain some of these phenotypic features
475 of ODG, and consistent with other reports suggesting that dysregulation of OPCs or OPC-like cells are
476 amongst the early changes in experimental models of gliomagenesis (2, 41).
477
478 There are some notable differences between the work reported by Yang, et al. (13), however, and our
479 studies. One difference is that the prior study used HOG cells that, despite their historic name, do not
480 carry the ODG-defining genetic features of 1p19q loss or *CIC* mutation; similarly the Pdgfra-
481 amplified/overexpressed mouse glioma model used is more akin to an RTK-driven GBM than it is to
482 ODG. In deploying the BT-88 and BT-54 models (which genetically and phenotypically faithfully
483 recapitulate ODG), our work may be closer to clinical relevance for ODG. Another difference is that our
484 studies also further clarify the early neuronal-glial fate decision effects of NSCs, with the bias away from
485 neuronal fates and toward glial fates in the setting of CIC loss. Most importantly, however, we now
486 identify *Ets* de-repression as a key mechanism underlying much of the phenotypic effects of Cic loss in
487 NSCs.

488

489 Our observation that *DN-Etv5* alone can abrogate so much of the pro-proliferative and pro-OPC
490 phenotype resulting from *Cic* loss was somewhat unexpected. In support of a role specifically for Etv5,
491 our observation that it is the most upregulated factor upon Cic loss, our Etv5 overexpression studies (in
492 vivo and in vitro), and our in vitro Etv5 siRNA experiments all lend independent support pointing to the
493 requirement for this particular Ets factor. However, we do not exclude that other Ets factors such as
494 Etv4 may also contribute. The dominant negative construct may not be entirely specific for inhibiting
495 Etv5 alone; such cross-reactivity has been reported with similar approaches, and further experiments
496 would be required to dissect the relative contribution of different Pea3 factors or other subfamilies of the
497 Ets genes. Nevertheless, the identification of this family of genes as a likely mediator is salient to the
498 development of future therapeutic strategies for ODG. Although it is thought that transcription factors
499 are difficult to target, reports of inhibition of other Ets factors either through peptidomimetic or small
500 molecule approaches (42-44) lend hope that Etv5 could potentially be inhibited for clinical benefit.

501

502 Finally, although our findings are relevant to ODG biology, it is recognized that our studies do not directly
503 model the genesis of ODG. Indeed, despite the increase in proliferation observed in Cic-null cells, no
504 tumors were detected when following for up to one year after *Cre* electroporation of the *Cic* floxed mice
505 (data not shown) – in keeping with the concept that several collaborating genetic hits are necessary for
506 oncogenic transformation. Our *Cic* conditional knockout mice, however, will be a useful tool for a future
507 more refined cell type- and stage-specific deletion of *Cic* along with the introduction of other mutations
508 such as of *IDH1*(R132H) (45). We conceptualize *IDH1/2* mutations as a first event in ODG, causing
509 epigenetic changes that that serve to expand the potential pool of cells vulnerable to transformation,
510 with second-hit loss of *CIC* serving to dysregulate proliferation, bias cells to oligodendroglial lineage,
511 and delay them in an immature state. Additional studies using experimental models and human ODG
512 samples are needed to further dissect the relationship of *CIC* mutation to *IDH* mutation. Although one
513 recent study used single-cell RNA-Seq to examine ODG cell subpopulations and did not detect any
514 differences between ODG cells with and without *CIC* mutation aside from the increased expression of

515 PEA3 Ets factors, the number of cells analyzed was limiting for resolution of cell type specific
516 differences, and functional studies had not been performed (46). Similar approaches with larger cell
517 numbers might provide further insight into the biology of ODG with respect to *CIC*.
518
519 In summary, we provide evidence that Cic regulates proliferation, fate decisions, and differentiation in
520 neural stem cells, with loss particularly expanding the OPC population. Furthermore, our findings
521 indicate that disruption of the Cic-Etv axis (with abnormal de-repression of *Etv5* downstream of *Cic* loss)
522 is central to the biology of ODG.
523
524

525 **METHODS**

526

527 **Mice**

528

529 CD1 outbred mice (Jackson Labs) were used for Cic expression analyses.

530

531 *Cic* conditional knockout (*Cic*-CKO) mice were generated at Taconic Artemis by homologous
532 recombination to flank Cic exons 2-11 with loxP sites. The exons targeted are 2-11 of *Cic* short form,
533 transcript variant 1, NM_027882.4 (equivalent to exons 3-12 of the *Cic* long form, NM_001302811.1,
534 Cic transcript variant 4). The targeting vector was generated using clones from the C57BL/6J RPCIB-
535 731 BAC library, and consisted of a 4.0 kb 5' flanking arm, neomycin resistance cassette (flanked by
536 FRT sites), 5.5 kb loxP-flanked region, a puromycin resistance cassette (flanked by F3 sites), and 6.0
537 kb 3' flanking arm. After homologous recombination in C57BL/6N Tac ES cells, generation of chimeric
538 animals, and germline transmission, Neo^R and $Puro^R$ cassettes were removed via Flp recombination by
539 breeding with a Flp deleter line. The
540 final CIC-CKO allele carries loxP sites in introns 1 and 11, and single residual FRT and F3 sites.
541 Expression of Cre recombinase results in deletion of exons 2-11 and frameshifting of the remaining CIC-
542 S exons 12-20. Genotyping primers were as follows: CIC 5' flanking region (192 bp wt, 348 bp CKO
543 allele) 5'- AGG AGG TTG TTA CTC GCT ATG G -3' (forward) and 5'- CTG ATG TCC TAA GAC CTT
544 TAC AAG G -3' (reverse); CIC 3' flanking region (273 bp wt, 410 bp CKO) 5' – CTG TGT CAC TGT
545 CTG CCT TCC -3' (forward) and 5' – TGG GTA ATA CCA CCG TGC C – 3 (reverse)'.

546

547 *FoxG1-cre* mice (Jackson Labs) were bred to *Cic*-CKO mice to generate telencephalic CIC knockouts
548 and littermate controls. After euthanasia, dissected brains were processed for histology, western
549 blotting, or cell culture. Knockout in tissue or cells post-cre was confirmed by Q-RT-PCR using
550 primer/probe sets for CIC (Applied Biosystems) and by Western blotting with anti-Cic.

551

552 In all mouse experiments, the morning of vaginal plug was designated embryonic day 0.5 (E0.5). Both
553 males and females were used.
554
555 **In utero electroporation**
556 In utero electroporation was performed as described previously [1] using the following plasmids:
557 pLKO.1-Cic shRNA (Sigma, TRCN0000304642; 5'-CCG GAG CGG GAG AAG GAC CAT ATT CCT
558 CGA GGA ATA TGG TCC TTC TCC CGC TTT TTT G-3'), pLKO.1-non-targeting shRNA (Sigma; 5'-
559 CCT AAG GTT AAG TCG CCC TCG CTC GAG CGA GGG CGA CTT AAC CTT AGG -3'), pCIG2-Cre
560 (which contains Cre-IRES-GFP), pCIC-ETV5 (which contains Etv5-IRES-mCherry), Super piggyBac
561 Transposase (Systems Biosciences, SBI), and piggyBac cargo vector PB513B-1 (SBI) into which
562 cDNAs were cloned for Turbo-Cre and Etv5. The DN-ETV5 consists of an *Etv5-EnR* fusion (gift of Dr.
563 Carol Schuurmans) cloned into the piggyBac construct modified to contain the CAG promoter and GFP-
564 luciferase. DNA was prepared with Endo-free DNA kit (Qiagen) and was injected at 1.5 µg/µl into the
565 telencephalic vesicles of embryos in time-staged pregnant females using a Femtojet 4i microinjector
566 (Eppendorf) then followed by electrical pulses (6 x 43 V, 950 ms interval) applied by platinum tweezer-
567 style electrodes (7 mm, Protech) using a BTX square wave generator (Harvard Apparatus). Post-
568 procedure, embryos were allowed to develop until the time of harvesting. EdU (50 mg/ml in PBS) was
569 injected intraperitoneally into the pregnant dam 30 minutes prior to euthanasia.
570
571 **Neural stem cell culture**
572 The VZ of E15 brains were dissected, and tissue was dissociated to single cells using Accumax (EMD
573 Millipore). Cells were grown at 37°C, 5% CO_2 in low-adhesion tissue culture flasks (Sarstedt) in mouse
574 neural stem cell (mNSC) media consisting of NeuroCult Proliferation media (Stem Cell Technologies)
575 supplemented with heparin, epidermal growth factor (EGF 20 ng/mL; Peprotech), and fibroblast growth
576 factor (FGF 20 ng/mL; Peprotech). When spheres reached 100–200 µm in diameter, cells were split
577 using Accumax and re-plated at 20,000 cells/mL.
578

579 **Transfection of cultured cells**

580 1-4 x 10^6 dissociated cells were re-suspended in 100 µL of Amaxa Mouse NSC Nucleofector Solution
581 (VPG-1004, Lonza) with 5 µg of plasmid DNA. Nucleofection was performed with a Nucleofector II
582 Device (Amaxa) using the A-033 program. Cells were returned to mouse neural stem cell media for
583 further expansion/selection. For siRNA-mediated Etv5 knockdown, cells were transfected with 50
584 nM Etv5 or Etv4 ON-TARGET Plus SMARTpool siRNAs (Dharmacon) using Lipofectamine 3000
585 reagent per manufacturer's protocol. Cells were assayed 48hrs hours post-transfection.

586

587 **Trypan Assay**

588 150,000 cells were seeded per T25 flask in mNSC media and counted after 72 hours on a TC20 cell
589 counter (Biorad) using Trypan blue stain (Thermo). Both dead and live cells were counted.

590

591 **Paired cell assay**

592 Dissociated cells were plated at 1,000 cells/ml in mNSC media on dishes coated with CTS CELLstart
593 (Thermo). After 20 hrs, cells were fixed in 4% PFA and immunostained for Ki67. Pairs were scored as
594 symmetric proliferative if both daughter nuclei were Ki67+, symmetric differentiative if both were Ki67-,
595 and asymmetric if one nucleus was Ki67+ and the other Ki67-.

596

597 **Neural Colony-Forming Cell Assay**

598 Cells in semi-solid media were prepared using the Neurocult NCFC Assay Kit (Stem Cell Technologies)
599 per manufacturer's protocol. Cells were plated at a density of 1,650 cells/ml using 1.5 ml per 35 mm
600 culture dish. Dishes were replenished after 7 days with 60 µl of neural stem cell proliferation media
601 supplemented with heparin, EGF, and FGF. Sphere number and size were scored using a gridded
602 scoring dish (Stem Cell Technologies). 8-cell aggregates were used as the cut-off for scoring.

603

604 **Lineage-directed differentiation**

605 Neuronal Differentiation: NSCs were seeded in mNSC proliferation media (Stem Cell Technologies) on
606 coverslips coated with Poly-L-Ornitihine and Laminin. After 24 hrs, media was replaced with Neurobasal
607 Media, 2% B-27, 2mM GlutaMAX-I (Thermo). After 4 more days dibutyryl cAMP (Sigma) was added
608 daily to a final concentration of 0.5 mM.
609 Oligodendroglial Differentiation: NSCs were seeded on coverslips coated with Poly-L-Ornitihine and
610 Laminin. After 24 hrs, media was replaced with Neurobasal media, 2% B-27, GlutaMAX-I, 30 ng/mL
611 3,3',5-Triiodo-L-thyronine sodium (Sigma).
612 Astrocyte Differentiation: NSCs were seeded on coverslips coated with Geltrex (Thermo). After 24 hrs,
613 media was replaced with DMEM, 1% N2-Supplement, 2mM GlutaMAX™-I, 1% FBS.
614
615 **Immunostaining**
616 Tissue was fixed overnight in 4% PFA, cryoprotected in 30% sucrose/PBS, and embedded in Tissue-
617 Tek O.C.T. (Sakura Finetek) prior to cutting 6 µm cryosections on Superfrost Plus slides (VWR).
618 Cultured cells grown on coverslips were fixed for 20 minutes in 4% PFA then rinsed in PBS.
619 Permeabilization was performed with 1× TBST (Tris-buffered saline: 25 mM Tris, 0.14 M NaCl, 0.1%
620 Triton X-100) for 15 min at room temperature (RT). 3% goat or horse serum in TBST x 30 min was used
621 for block. Primary antibodies applied for 1 hr at RT or O/N at 4°C in block. Alexa Fluor secondary
622 antibodies were applied at 1:500 dilution for 1 hour RT. Nuclei were counterstained in 4′,6-diamidino-2-
623 phenylindole (DAPI; Santa Cruz) and mounted with FluorSave Reagent (Calbiochem). For
624 immunostaining of tissue sections when two or more primary antibodies were from the same host
625 species and for comparison of cell-type specific CIC expression, the Opal 4-colour IHC kit (PerkinElmer)
626 was used per manufacturer's protocol.
627
628 **Western blotting**
629 Cells/tissue was lysed in RIPA buffer (10 mM Tris-Cl pH 8, 1 mM EDTA, 1% Triton X-100, 0.1% sodium
630 deoxycholate, 0.1% SDS, 140 mM NaCl, 1 mM PMSF) with 1X Halt Protease and Phosphatase Inhibitor
631 Cocktail (Thermo). 20 µg protein lysate (50 µg in the case of CIC probing) was run on 4-12% Bis-Tris or

632 3-8% Tris-Acetate gels (Thermo). Protein was transferred to PVDF membranes in NuPAGE Transfer
633 Buffer (Thermo). Membranes were blocked in TBST with 5% powdered milk. Primary antibodies diluted
634 were applied for 1 hr at room temperature or overnight at 4°C. Horseradish peroxidase-coupled
635 secondary antibodies were applied for 1 hr at room temperature. Membranes were developed using
636 ECL Plus Western Blotting Reagent (GE Healthcare) and X-ray film.
637
638 **Transcriptional analysis**
639 Total RNA was extracted using AllPrep DNA/RNA/Protein Mini Kit (Qiagen) per manufacturer's protocol.
640 For each of 3 biologic replicates per condition, 100 ng RNA was subjected to nanoString analysis on
641 nCounter system (NanoString Technologies) using a custom gene expression codeset containing
642 neurodevelopmental and brain cancer associated genes, and 3 housekeeping genes. Data were
643 analyzed using nSolver software and exported to PRISM software for further statistical analyses.
644 Counts for Etv1, Etv4, and Etv5 were normalized to the average of 3 house-keeping genes (GAPDH,
645 Actin, Tubulin beta chain).
646
647 ***In situ* hybridization**
648 Digoxygenin (DIG)-labeled riboprobes were prepared using a 10x DIG-labeling kit (Roche), and ISH
649 was performed as described previously using probes for *GFP* and *Etv5* (17).
650
651 **Chromatin immunoprecipitation**
652 50 mg P6 mouse forebrain tissue was use per ChIP assay. ChIP was performed with the SimpleChip
653 Plus Kit with magnetic beads (Cell Signaling) per manufacturer's protocol with the following exceptions.
654 Tissue was disaggregated using a Dounce homogenizer. In place of micrococcal nuclease, shearing
655 was performed on a UCD Bioruptor on high power with intervals of 30 seconds on, 1 minute off for 30
656 minutes. 1.5 µl of anti-CIC (PA1-46018, Thermo) was used per IP reaction. Histone H3 antibody and
657 normal rabbit IgG were used as positive and negative controls, as supplied in the kit. PCR primers for

658 the ETV5 promoter region were: 5′-GGTGCAGGCCGAGGCCAGGG-3′ (For) and 5′-
659 CATTGACCAATCAGCACCGG-3′ (Rev).
660
661 **Image Analysis**
662 Coronal sections at the level of the anterior commissure were used in all quantitations of cell populations
663 and staining intensities in the dorsal cerebral cortex and corpus callosum. Slides were imaged on
664 AxioObserver fluorescence microscope (Zeiss). Images were processed using CS6 Photoshop software
665 (Adobe) for orientation, false colorization, and overlay/colocalization. Enumeration of cells positive for
666 cytoskeletal, cytoplasmic or membrane proteins was performed manually by counting positive cells
667 using the Photoshop CS6 counting tool. Quantitation of CIC nuclear staining intensity and MBP staining
668 density was performed using FIJI software (47) as follows. Images were first processed using Gaussian
669 blur, then background subtracted. Default threshold limits were used in the threshold tool. Images were
670 converted to binary and watershed was run to separate clumped cells. Nuclear staining was quantitated
671 by using the analysing particles option with separate cut-offs set for each antibody used. For quantitation
672 of MBP expression on tissue sections, FIJI was used by drawing regions of interest on the lateral corpus
673 callosum (cingulum), and the mean integrated density in the regions of interest was calculated.
674

675 **Intracranial BTIC xenografts and Bioluminescence imaging**

676 1×10^5 BT88 cells stably transfected with CIC-GFP-Luciferase or DNETV5-GFP or respective empty
677 vectors were stereotactically implanted into the right striata of 6- to 8-week-old NOD/SCID mice. 6 weeks
678 post-implantation, tumour burden was measured either by bioluminescence imaging using IVIS
679 Spectrum In Vivo Imaging System (Xenogen) and/or by histology from euthanized animals. Mice were
680 anaesthetized under isoflurane and intraperitoneal injection of XenoLight D-Luciferin (PerkinElmer) was
681 administered at a dose of 150mg/kg body weight. Acquisition of bioluminescence images was performed
682 10 min post-injection. Analysis was performed using Living Image Software by measurement of photon
683 counts (photon/s/cm^2) with a region of interest drawn around the bioluminescence signal.

684

685 **Statistics**

686 Data are represented as mean ± SD from at least 3 biologic replicates for experiments. Comparisons
687 between experimental and control samples were made using 2-tailed t-test or, when there were more
688 than 2 group, using ANOVA. Tukey's procedure was applied post-hoc to correct for multiple
689 comparisons during multiple pairwise analyses (e.g. differential Cic expression among cell types).
690 Bonferroni post-hoc correction was applied for statistical analysis of data from NanoString assays.
691 Statistical analyses were performed using Prism sofware (Graphpad).

692

693 **Study Approval**

694 Animal use was approved by the University of Calgary Animal Care Committee (protocol AC16-0266)
695 in compliance with the Guidelines of the Canadian Council of Animal Care.

696

697 **AUTHOR CONTRIBUTIONS**

698 Conceptualization, JAC, STA; Methodology, JAC, CS, STA; Investigation, STA, ADR, RD, LF, MJC,
699 MA, WW, SOL; Acquisition, Analyses and Interpretation of data, JAC, STA; Writing – Original Draft,
700 JAC, STA; Writing – Review & Editing, JAC, SC, JGC, SMR, MAM, WW, RD, SOL; Funding Acquisition,
701 JAC, JGC, CS; Resources, LA, MA, CS; Supervision, JAC, CS, JGC, SMR.

702

703 **ACKNOWLEDGEMENTS**

704 This work was funded by Canadian Institutes for Health Research (JAC), Cancer Research Society (CS,
705 JAC), Alberta Cancer Foundation (STA, ADR, LF, JGC), Alberta Innovates Health Solutions (JAC, CS).

706

707 **COMPETING FINANCIAL INTERESTS**

708 The authors have no competing financial interests to declare.

709
710

711 **REFERENCES**
712

713 1. Reifenberger G, Kros JM, Louis DN, and Collins VP. In: Louis DN, Ohgaki H, Wiestler OD,
714 and Cavenee WK eds. *WHO Classification of Tumours of the Central Nervous System*. Lyon:
715 International Agency for Research on Cancer (IARC); 2016:54-62.
716 2. Persson AI, Petritsch C, Swartling FJ, Itsara M, Sim FJ, Auvergne R, et al. Non-stem cell origin
717 for oligodendroglioma. *Cancer cell.* 2010;18(6):669-82.
718 3. Yip S, Butterfield YS, Morozova O, Chittaranjan S, Blough MD, An J, et al. Concurrent CIC
719 mutations, IDH mutations, and 1p/19q loss distinguish oligodendrogliomas from other cancers.
720 *The Journal of pathology.* 2012;226(1):7-16.
721 4. Bettegowda C, Agrawal N, Jiao Y, Sausen M, Wood LD, Hruban RH, et al. Mutations in CIC
722 and FUBP1 contribute to human oligodendroglioma. *Science.* 2011;333(6048):1453-5.
723 5. Cancer Genome Atlas Research N, Brat DJ, Verhaak RG, Aldape KD, Yung WK, Salama SR,
724 et al. Comprehensive, Integrative Genomic Analysis of Diffuse Lower-Grade Gliomas. *N Engl*
725 *J Med.* 2015;372(26):2481-98.
726 6. Jimenez G, Shvartsman SY, and Paroush Z. The Capicua repressor - a general sensor of RTK
727 signaling in development and disease. *Journal of cell science.* 2012;125(Pt 6):1383-91.
728 7. Lohr U, Chung HR, Beller M, and Jackle H. Antagonistic action of Bicoid and the repressor
729 Capicua determines the spatial limits of Drosophila head gene expression domains. *Proc Natl*
730 *Acad Sci U S A.* 2009;106(51):21695-700.
731 8. Ajuria L, Nieva C, Winkler C, Kuo D, Samper N, Andreu MJ, et al. Capicua DNA-binding sites
732 are general response elements for RTK signaling in Drosophila. *Development.*
733 2011;138(5):915-24.
734 9. Grimm O, Zini VS, Kim Y, Casanova J, Shvartsman SY, and Wieschaus E. Torso RTK controls
735 Capicua degradation by changing its subcellular localization. *Development.* 2012;139(21):3962-
736 8.
737 10. Astigarraga S, Grossman R, Diaz-Delfin J, Caelles C, Paroush Z, and Jimenez G. A MAPK
738 docking site is critical for downregulation of Capicua by Torso and EGFR RTK signaling. *The*
739 *EMBO journal.* 2007;26(3):668-77.
740 11. Lim B, Samper N, Lu H, Rushlow C, Jimenez G, and Shvartsman SY. Kinetics of gene
741 derepression by ERK signaling. *Proc Natl Acad Sci U S A.* 2013;110(25):10330-5.
742 12. Dissanayake K, Toth R, Blakey J, Olsson O, Campbell DG, Prescott AR, et al.
743 ERK/p90(RSK)/14-3-3 signalling has an impact on expression of PEA3 Ets transcription
744 factors via the transcriptional repressor capicua. *The Biochemical journal.* 2011;433(3):515-25.
745 13. Yang R, Chen LH, Hansen LJ, Carpenter AB, Moure CJ, Liu H, et al. Cic Loss Promotes
746 Gliomagenesis via Aberrant Neural Stem Cell Proliferation and Differentiation. *Cancer Res.*
747 2017;77(22):6097-108.
748 14. Lu HC, Tan Q, Rousseaux MW, Wang W, Kim JY, Richman R, et al. Disruption of the
749 ATXN1-CIC complex causes a spectrum of neurobehavioral phenotypes in mice and humans.
750 *Nature genetics.* 2017;49(4):527-36.
751 15. Graham V, Khudyakov J, Ellis P, and Pevny L. SOX2 functions to maintain neural progenitor
752 identity. *Neuron.* 2003;39(5):749-65.
753 16. Faedo A, Borello U, and Rubenstein JL. Repression of Fgf signaling by sprouty1-2 regulates
754 cortical patterning in two distinct regions and times. *The Journal of neuroscience : the official*
755 *journal of the Society for Neuroscience.* 2010;30(11):4015-23.
756 17. Li S, Mattar P, Dixit R, Lawn SO, Wilkinson G, Kinch C, et al. RAS/ERK signaling controls
757 proneural genetic programs in cortical development and gliomagenesis. *The Journal of*
758 *neuroscience : the official journal of the Society for Neuroscience.* 2014;34(6):2169-90.

759 18. Kriegstein A, and Alvarez-Buylla A. The glial nature of embryonic and adult neural stem cells.
760 *Annual review of neuroscience.* 2009;32:149-84.
761 19. Lim DA, and Alvarez-Buylla A. The Adult Ventricular-Subventricular Zone (V-SVZ) and
762 Olfactory Bulb (OB) Neurogenesis. *Cold Spring Harb Perspect Biol.* 2016;8(5).
763 20. Lu QR, Sun T, Zhu Z, Ma N, Garcia M, Stiles CD, et al. Common developmental requirement
764 for Olig function indicates a motor neuron/oligodendrocyte connection. *Cell.* 2002;109(1):75-
765 86.
766 21. Zhou Q, Choi G, and Anderson DJ. The bHLH transcription factor Olig2 promotes
767 oligodendrocyte differentiation in collaboration with Nkx2.2. *Neuron.* 2001;31(5):791-807.
768 22. Fores M, Simon-Carrasco L, Ajuria L, Samper N, Gonzalez-Crespo S, Drosten M, et al. A new
769 mode of DNA binding distinguishes Capicua from other HMG-box factors and explains its
770 mutation patterns in cancer. *PLoS genetics.* 2017;13(3):e1006622.
771 23. Jimenez G, Guichet A, Ephrussi A, and Casanova J. Relief of gene repression by torso RTK
772 signaling: role of capicua in Drosophila terminal and dorsoventral patterning. *Genes &*
773 *development.* 2000;14(2):224-31.
774 24. Lee CJ, Chan WI, Cheung M, Cheng YC, Appleby VJ, Orme AT, et al. CIC, a member of a
775 novel subfamily of the HMG-box superfamily, is transiently expressed in developing granule
776 neurons. *Brain Res Mol Brain Res.* 2002;106(1-2):151-6.
777 25. Kawamura-Saito M, Yamazaki Y, Kaneko K, Kawaguchi N, Kanda H, Mukai H, et al. Fusion
778 between CIC and DUX4 up-regulates PEA3 family genes in Ewing-like sarcomas with
779 t(4;19)(q35;q13) translocation. *Human molecular genetics.* 2006;15(13):2125-37.
780 26. Hebert JM, and McConnell SK. Targeting of cre to the Foxg1 (BF-1) locus mediates loxP
781 recombination in the telencephalon and other developing head structures. *Developmental*
782 *biology.* 2000;222(2):296-306.
783 27. Sugiarto S, Persson AI, Munoz EG, Waldhuber M, Lamagna C, Andor N, et al. Asymmetry-
784 defective oligodendrocyte progenitors are glioma precursors. *Cancer cell.* 2011;20(3):328-40.
785 28. Finzsch M, Stolt CC, Lommes P, and Wegner M. Sox9 and Sox10 influence survival and
786 migration of oligodendrocyte precursors in the spinal cord by regulating PDGF receptor alpha
787 expression. *Development.* 2008;135(4):637-46.
788 29. Kang P, Lee HK, Glasgow SM, Finley M, Donti T, Gaber ZB, et al. Sox9 and NFIA coordinate
789 a transcriptional regulatory cascade during the initiation of gliogenesis. *Neuron.* 2012;74(1):79-
790 94.
791 30. Stolt CC, Lommes P, Sock E, Chaboissier MC, Schedl A, and Wegner M. The Sox9
792 transcription factor determines glial fate choice in the developing spinal cord. *Genes &*
793 *development.* 2003;17(13):1677-89.
794 31. Lee Y, Fryer JD, Kang H, Crespo-Barreto J, Bowman AB, Gao Y, et al. ATXN1 protein family
795 and CIC regulate extracellular matrix remodeling and lung alveolarization. *Developmental cell.*
796 2011;21(4):746-57.
797 32. Padul V, Epari S, Moiyadi A, Shetty P, and Shirsat NV. ETV/Pea3 family transcription factor-
798 encoding genes are overexpressed in CIC-mutant oligodendrogliomas. *Genes Chromosomes*
799 *Cancer.* 2015;54(12):725-33.
800 33. Crespo-Barreto J, Fryer JD, Shaw CA, Orr HT, and Zoghbi HY. Partial loss of ataxin-1 function
801 contributes to transcriptional dysregulation in spinocerebellar ataxia type 1 pathogenesis. *PLoS*
802 *genetics.* 2010;6(7):e1001021.
803 34. Li X, Newbern JM, Wu Y, Morgan-Smith M, Zhong J, Charron J, et al. MEK Is a Key
804 Regulator of Gliogenesis in the Developing Brain. *Neuron.* 2012;75(6):1035-50.
805 35. Kelly JJ, Blough MD, Stechishin OD, Chan JA, Beauchamp D, Perizzolo M, et al.
806 Oligodendroglioma cell lines containing t(1;19)(q10;p10). *Neuro Oncol.* 2010;12(7):745-55.

807 36. Davoli T, Xu AW, Mengwasser KE, Sack LM, Yoon JC, Park PJ, et al. Cumulative
808 haploinsufficiency and triplosensitivity drive aneuploidy patterns and shape the cancer genome.
809 *Cell.* 2013;155(4):948-62.
810 37. Lam YC, Bowman AB, Jafar-Nejad P, Lim J, Richman R, Fryer JD, et al. ATAXIN-1 interacts
811 with the repressor Capicua in its native complex to cause SCA1 neuropathology. *Cell.*
812 2006;127(7):1335-47.
813 38. Rousseaux MWC, Tschumperlin T, Lu HC, Lackey EP, Bondar VV, Wan YW, et al. ATXN1-
814 CIC Complex Is the Primary Driver of Cerebellar Pathology in Spinocerebellar Ataxia Type 1
815 through a Gain-of-Function Mechanism. *Neuron.* 2018;97(6):1235-43 e5.
816 39. Cairncross G, and Jenkins R. Gliomas with 1p/19q codeletion: a.k.a. oligodendroglioma.
817 *Cancer J.* 2008;14(6):352-7.
818 40. Shoshan Y, Nishiyama A, Chang A, Mork S, Barnett GH, Cowell JK, et al. Expression of
819 oligodendrocyte progenitor cell antigens by gliomas: implications for the histogenesis of brain
820 tumors. *Proc Natl Acad Sci U S A.* 1999;96(18):10361-6.
821 41. Liu C, Sage JC, Miller MR, Verhaak RG, Hippenmeyer S, Vogel H, et al. Mosaic analysis with
822 double markers reveals tumor cell of origin in glioma. *Cell.* 2011;146(2):209-21.
823 42. Butler MS, Roshan-Moniri M, Hsing M, Lau D, Kim A, Yen P, et al. Discovery and
824 characterization of small molecules targeting the DNA-binding ETS domain of ERG in prostate
825 cancer. *Oncotarget.* 2017;8(26):42438-54.
826 43. Pop MS, Stransky N, Garvie CW, Theurillat JP, Hartman EC, Lewis TA, et al. A small
827 molecule that binds and inhibits the ETV1 transcription factor oncoprotein. *Mol Cancer Ther.*
828 2014;13(6):1492-502.
829 44. Wang X, Qiao Y, Asangani IA, Ateeq B, Poliakov A, Cieslik M, et al. Development of
830 Peptidomimetic Inhibitors of the ERG Gene Fusion Product in Prostate Cancer. *Cancer cell.*
831 2017;31(4):532-48 e7.
832 45. Pirozzi CJ, Carpenter AB, Waitkus MS, Wang CY, Zhu H, Hansen LJ, et al. Mutant IDH1
833 Disrupts the Mouse Subventricular Zone and Alters Brain Tumor Progression. *Mol Cancer Res.*
834 2017.
835 46. Tirosh I, Venteicher AS, Hebert C, Escalante LE, Patel AP, Yizhak K, et al. Single-cell RNA-
836 seq supports a developmental hierarchy in human oligodendroglioma. *Nature.*
837 2016;539(7628):309-13.
838 47. Schindelin J, Arganda-Carreras I, Frise E, Kaynig V, Longair M, Pietzsch T, et al. Fiji: an open-
839 source platform for biological-image analysis. *Nat Methods.* 2012;9(7):676-82.

840

841

FIGURES

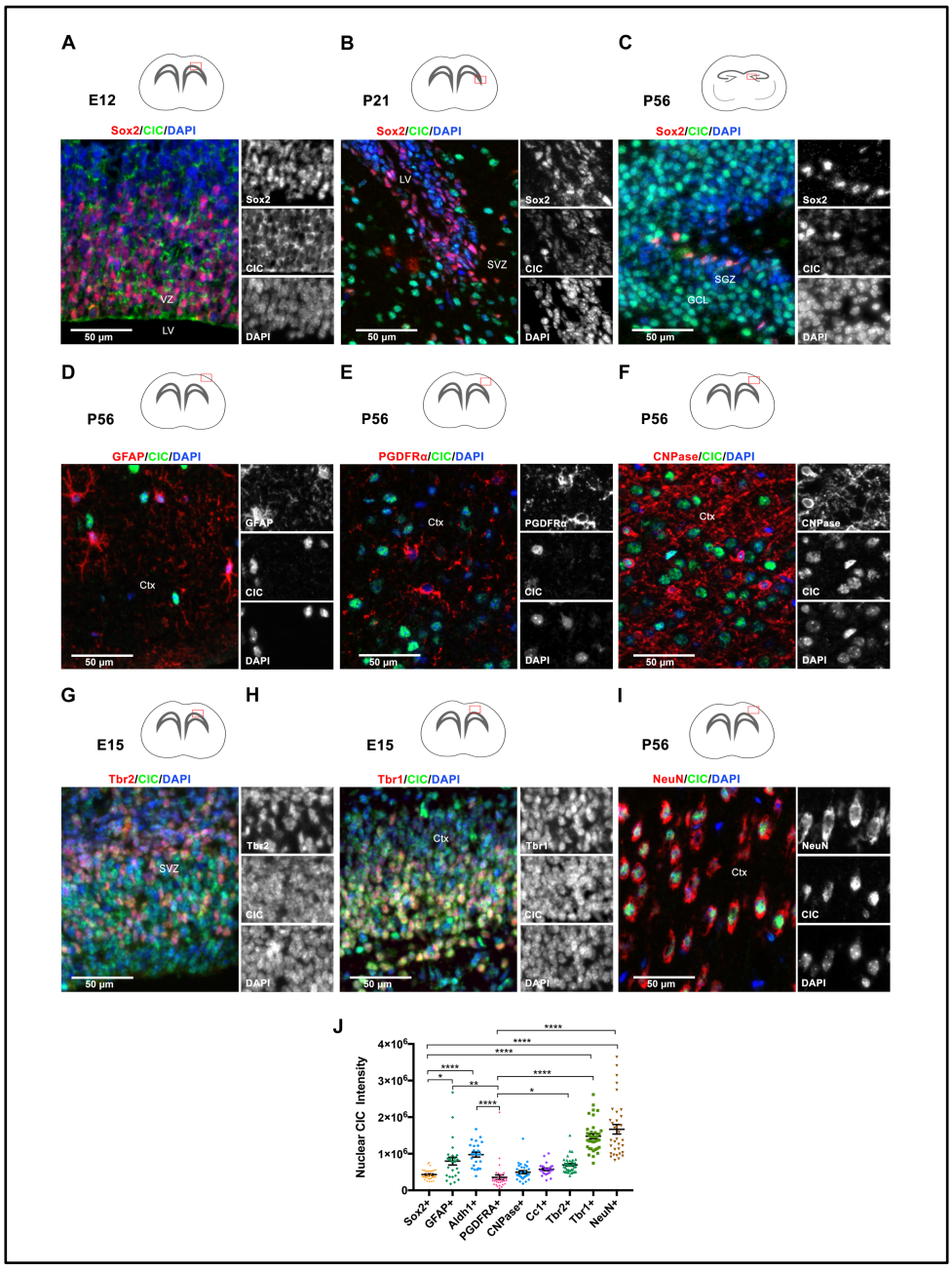

FIGURE 1: Differential Cic expression among cell types in the developing and mature brain. Representative images of immunofluorescence staining for Cic expression in Sox2+ stem cell populations in (A) E12 subventricular zone, (B) P56 hippocampal dentate gyrus subgranular zone, and (C) P56 subventricular zone. Cic expression in glial cells in the adult brain showing localization in (D) Gfap+ cortical astrocytes, (E) Pdgfra+ white matter OPCs, and (F) CNPase+ mature oligodendrocytes. Cic expression in cortical neuronal populations (G) E15 Tbr2+ early-born neurons in the SVZ and IZ, (H) E15 Tbr1+ late-born neurons in the cortical plate, and (I) adult post-mitotic NeuN+ cortical neurons. (J) Quantitation of Cic nuclear staining intensities, plotted for different brain cell types. Each point represents one cell quantitated. Results show quantitation from a minimum of 24 cells per marker from the boxed regions used for image analysis. All quantitation performed on P56 cortex except Tbr2 and Tbr1 which were analyzed at E15. Pairwise comparisons between cell types performed by ANOVA with Tukey's posthoc test. Data shown as mean ± SD. *p<0.05, **p<0.01, ****p<0.0001. LV–lateral ventricle, GCL–granule cell layer, SGZ–subgranular zone, SVZ–subventricular zone, Ctx–cortex.

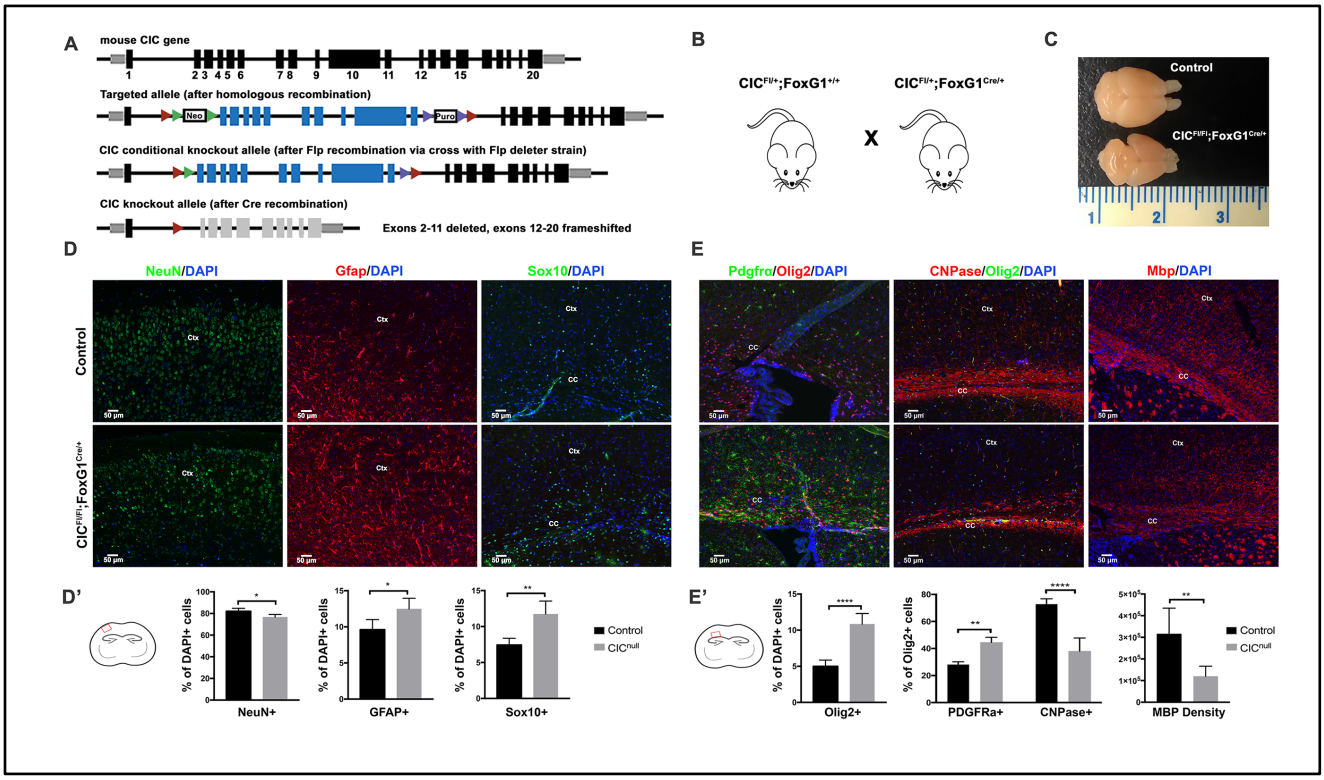

FIGURE 2: Forebrain-specific *Cic* deletion increases glial cells at the expense of neurons by P21 (A) Targeting strategy for Cic conditional knockout mice. Exon numbering is shown relative to Cic transcript variant 1. (B) Forebrain-deletion of Cic starting from E10.5 by crossing CIC-floxed line with FoxG1-cre. *Cic*$^{Fl/Fl}$*;FoxG1*$^{Cre/+}$ animals are compared with *Cic*$^{Fl/+}$*;FoxG*$^{Cre/+}$ or *Cic*$^{Fl/Fl}$*;FoxG1*$^{+/+}$ as controls. (C) Representative gross morphology of *Cic*-deleted and *Cic*-wildtype brains at P21. (D,D') Staining and quantitation of NeuN+, Gfap+, and Sox10+ cells in Cic-deleted (*Cic*$^{Fl/Fl}$*;FoxG1*$^{Cre/+}$) cortex vs control (*Cic*$^{Fl/Fl}$*;FoxG1*$^{+/+}$). (E,E') Staining and quantitation of Olig2+, Pdgfra+, and CNPase+ cells in lateral corpus callosum, and Mbp expression in lateral corpus callosum at P21. Results show quantitation from 5 mice per each group. Statistical analyses performed by unpaired t-test. Data shown as mean ± SD. *p<0.05, **p<0.01, ****p<0.0001. Ctx–cortex, CC–corpus callosum.

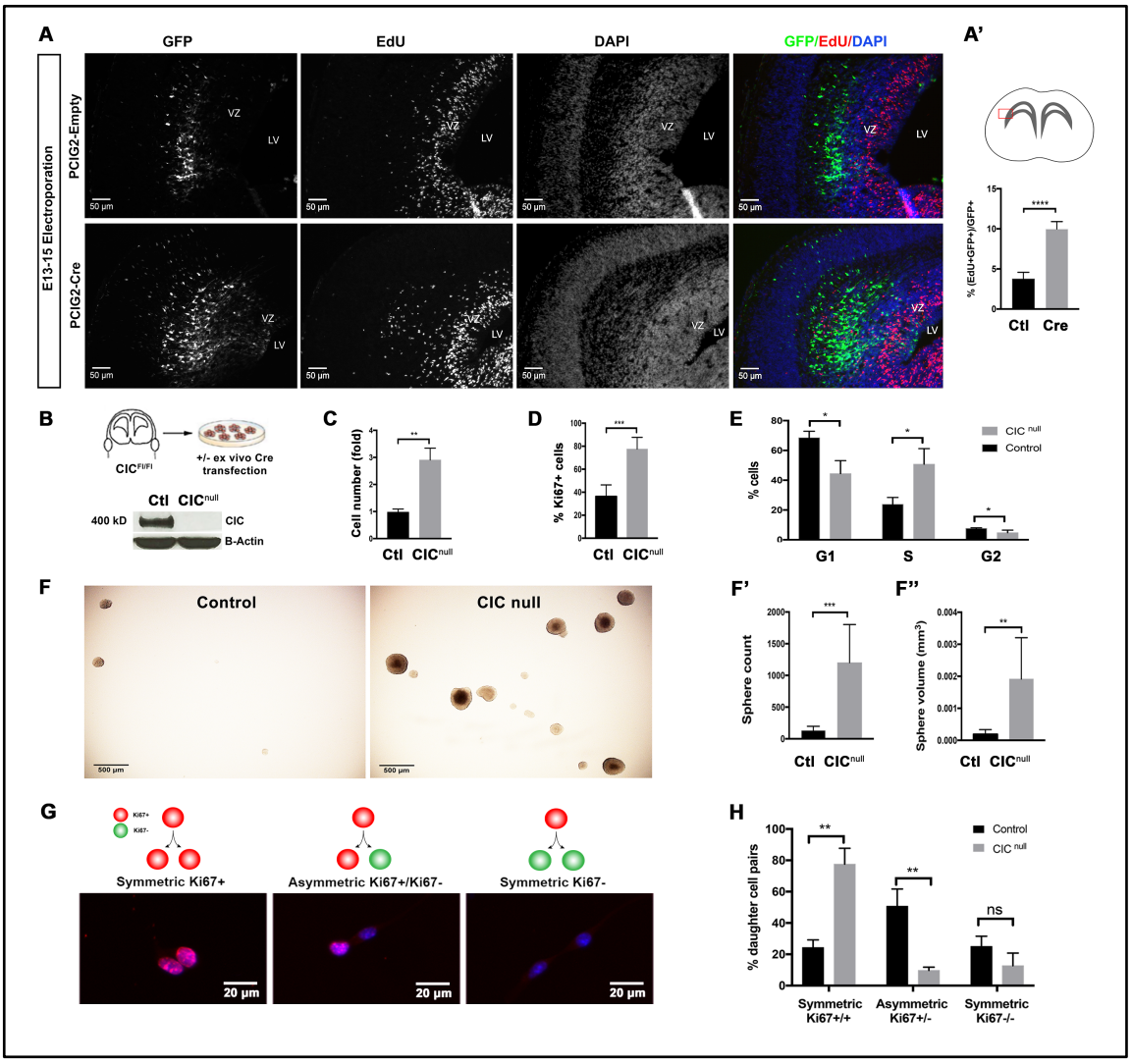

FIGURE 3: Cic deficiency increases proliferation and self-renewal of neural stem/progenitor cells. (A,A') EdU incorporation 48-hours after electroporation of *Cre* or control plasmid into VZ of E13 *Cic*-floxed embryos; boxed area indicates zone for imaging and quantitation (n ≥ 4 mice per group). (B) Generation of Cic-null cells and control cells from *Cic*-floxed cells via ex vivo transfection of Cre recombinase, and western blotting for validation of knockout. (C) Trypan blue assay, (D) Ki67 proliferation index, and (E) propidium iodide cell cycle analysis in cultured cells. (F) Neural colony forming assay with quantitation of (F') sphere number and (F'') sphere size. (G) Paired cell assay schematic and representative images with Ki67 immunostaining and (H) Quantitation of symmetric proliferative, asymmetric, and symmetric terminal divisions. Data shown as mean ± SD. Data from ≥ 3 biologic replicates per condition. Statistical analysis performed by unpaired t-test. ns-not significant, *p<0.05, **p<0.01, ***p<0.001, ****p<0.0001. VZ–ventricular zone, LV–lateral ventricle.

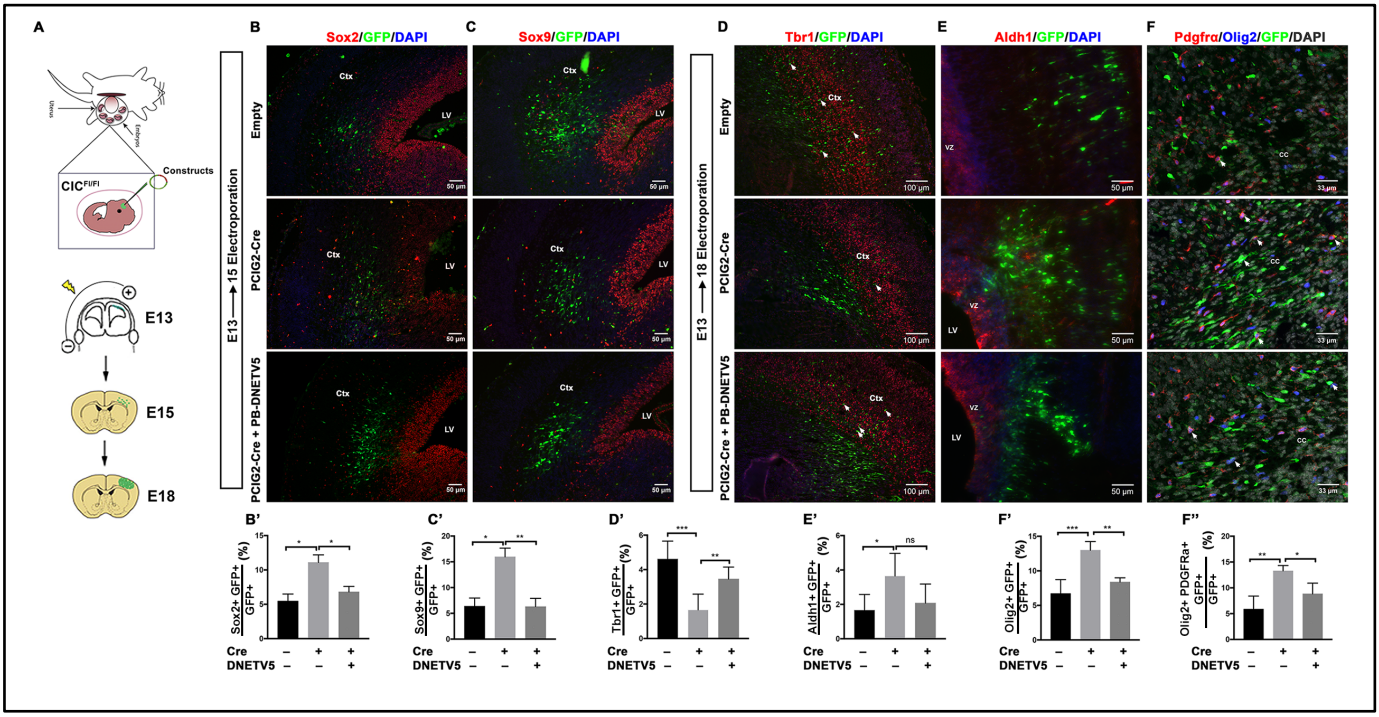

FIGURE 4: Deletion of *Cic* in the neurogenic period biases neural stem/progenitor cells to glial lineage selection. (A) Localized deletion of *Cic* in neural stem cells via *in-utero* electroporation into VZ cell of *Cic*-floxed embryos. Targeted cells carry a fluorescent marker and express either cre recombinase (Cre), dominant negative ETV5 (DNETV5), or not (Empty control), depending on the electroporated plasmid. Staining and quantitation of Sox2+ stem cells (B,B') and Sox9+ glioblasts (C,C') 2 days after E13 electroporation. Staining and quantitation of late-born Tbr1+ neurons, Aldh1+ astrocytes, Olig2+ oligodendrogial lineage cells, and Pdgfra+ oligodendrocyte precursors cells 5 days after E13 electroporation. Results show quantitation from 4 mice per group. Statistical analyses between control and experimental groups performed by ANOVA with Tukey's posthoc test. Data shown as mean ± SD. *p<0.05, **p<0.01, ***p<0.001, ns–not significant. Ctx–cortex, LV–lateral ventricle, VZ–ventricular zone.

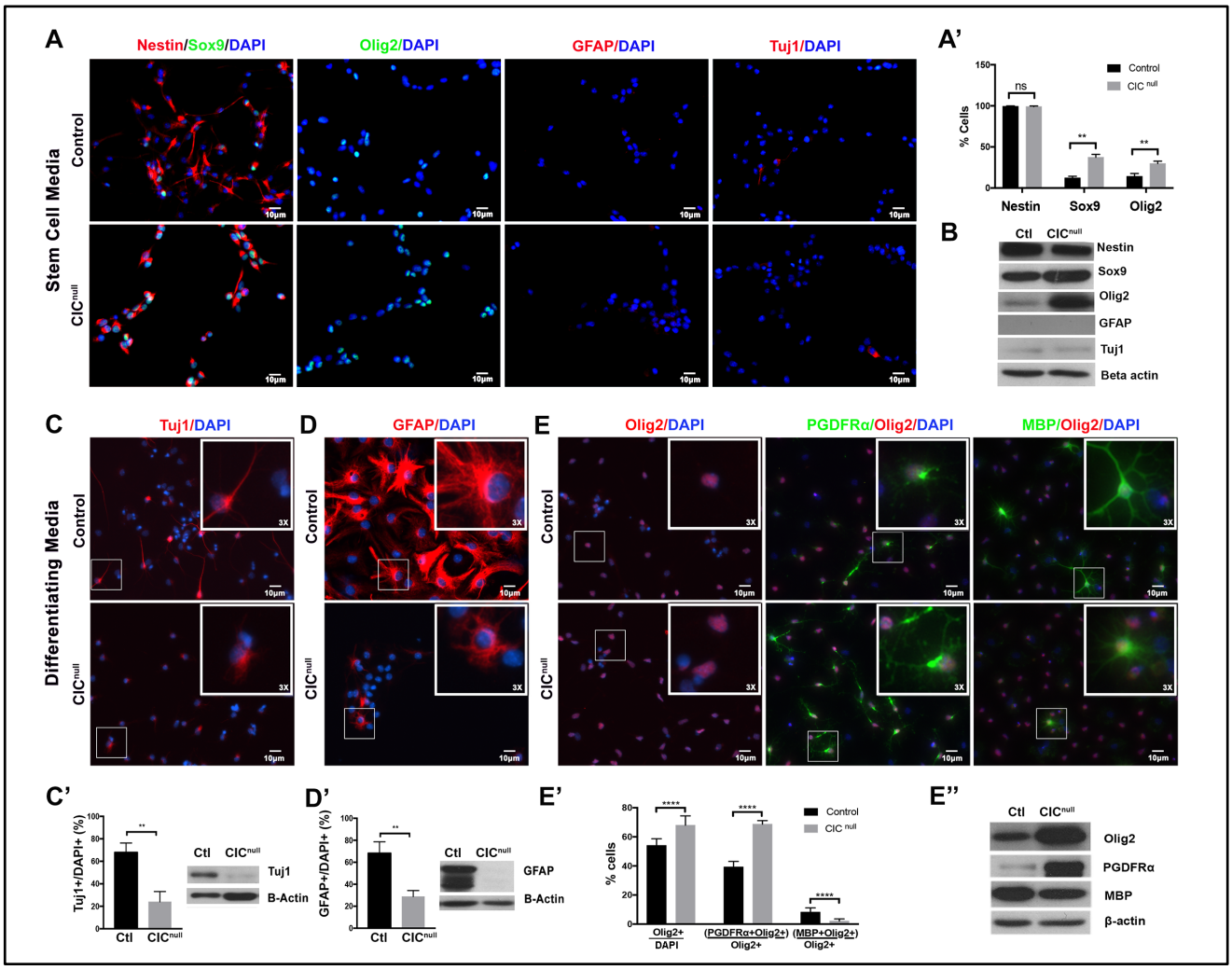

FIGURE 5: Cultured Cic null cells are oligodendrocyte lineage-biased. (A) Immunofluorescence and (B) Western blotting for Nestin, Sox9, Olig2, Gfap, and Tuj1 in Cic-null and control cells cultured in stem cell conditions. Responses of Cic-null and control cells to 10-day exposure to lineage-directed differentiation conditions for (C) neurons, (D) astrocytes, or (E) oligodendrocytes. Immunofluorescence quantitation of cell populations and western blotting of cells cultured in lineage-directed differentiation conditions for (C') neurons, (D') astrocytes, and (E', E'') stages of oligodendrocyte development. Data shown as mean ± SD. Data from ≥ 3 biologic replicates per condition. Statistical analysis performed by unpaired t-test. ns-not significant, **p<0.01, ****p<0.0001.

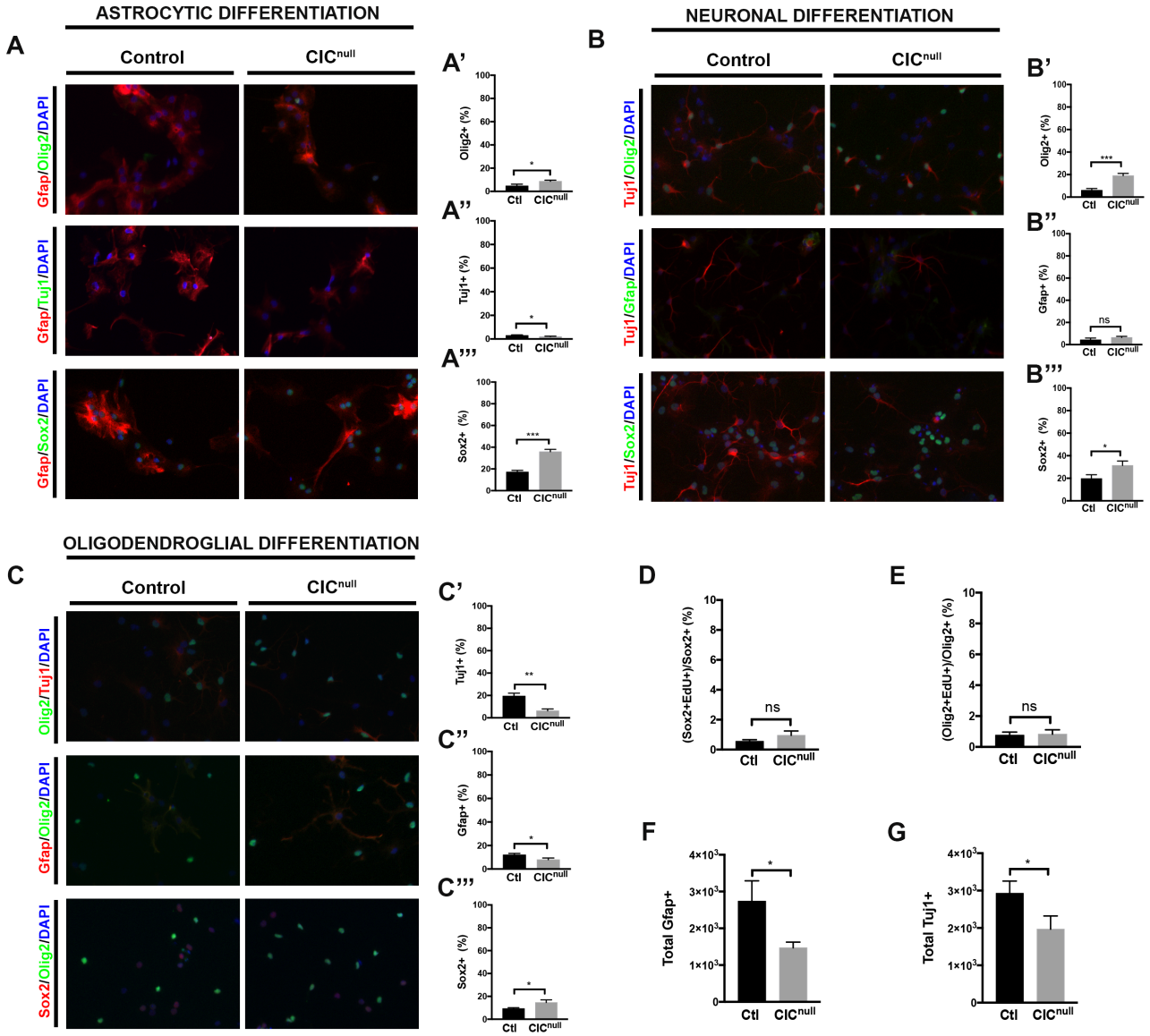

Figure 6: Alternate lineage selection of Cic null NSCs in response to extrinsic differentiation cues. (A) Under astrocytic promoting conditions, representative images of cultures stained for oligodendrocytes (Olig2+), neurons (Tuj1+) and stem cells (Sox2+); and (A',A'',A''') corresponding quantifications. (B) Under neuronal promoting conditions, representative images of cultures stained for oligodendrocytes (Olig2+), astrocytes (Gfap+) and stem cells (Sox2+); and (B',B'',B''') corresponding quantifications.(C) Under oligodendrocytic promoting conditions, representative images of cultures stained for neurons (Tuj1+), astrocytes (Gfap+) and stem cells (Sox2+); and (C',C'',C''') corresponding quantifications. (D) Percentage of Sox2+ cells positive for Edu incorporation after 10 days exposure to neuronal promoting conditions. (E) Percentage of Olig2+ positive for Edu incorporation after 10 days exposure to neuronal promoting conditions. (F) Absolute counts of Gfap+ cells/well after differentiating $4x10^3$ NSCs in astrocytic conditions for 10 days. (G) Absolute counts of Tuj1+ cells/well after differentiation $4x10^3$ NSCs in neuronal conditions for 10 days. Bars indicate mean±SD. ADC-Astrocytic differentiation condition, NDC-Neuronal differentiation condition, ODC-Oligodendroglial differentiation condition. ns – not significant, * $p<0.05$, ***$p<0.001$.

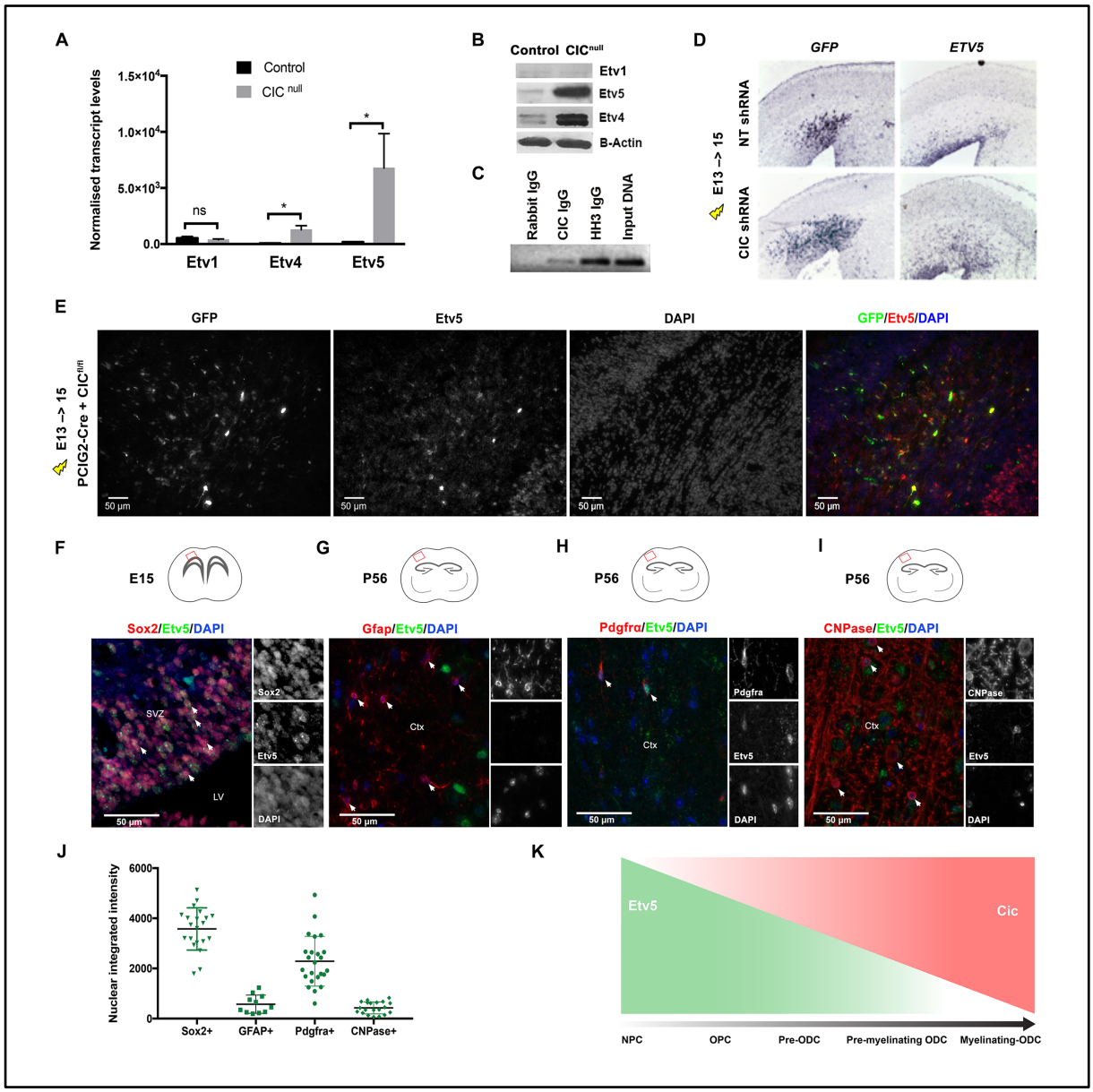

FIGURE 7: *Etv5* is a direct target of Cic transcriptional repression. *Etv1*, *Etv4*, and *Etv5* mRNA (A) and protein (B) levels in cultured CIC-null and -control cells after 48-hour exposure to oligodendrocytic differentiating conditions; transcript levels normalized to average of 3 (Actin, GAPDH, Tubulin beta chain) housekeeping genes. Data from n=3 biologic replicates. (C) ChIP-PCR for Cic at the *Etv5* promoter. (D) Electroporation of Cic shRNA or non-targeting (NT*)* shRNA at E13 followed by *in-situ* hybridization for *Etv5* and *GFP* at E15; *Etv5* transcripts are upregulated in areas of Cic knockdown. Data from n≥3 mice per group. (E) Immunofluorescence staining showing Etv5 and GFP protein expression 2 days after Cre electroporation into E13 VZ of *Cic*-floxed embryos. *Cic* deleted cells show increased Etv5 protein. (F-I, J) Differential Etv5 expression in (F) NSCs (Sox2+) at mid-neurogenesis, and in (G) astrocytes (Gfap+), (H) OPCs (Pdgfra+), and (I) mature oligodendrocytes (CNPase+) in P56 adult cortex. Each point represents one cell quantitated. Results show quantitation from ≥20 cells for each marker. Data shown as mean ± SD. Statistical analyses performed by unpaired t-test. *p<0.05. SVZ–subventricular zone, LV–lateral ventricle, Ctx–cortex. (K) Schematic depiction of relationship of Cic and Etv5 expression as neural stem cells differentiate to mature myelinating oligodendrocytes.

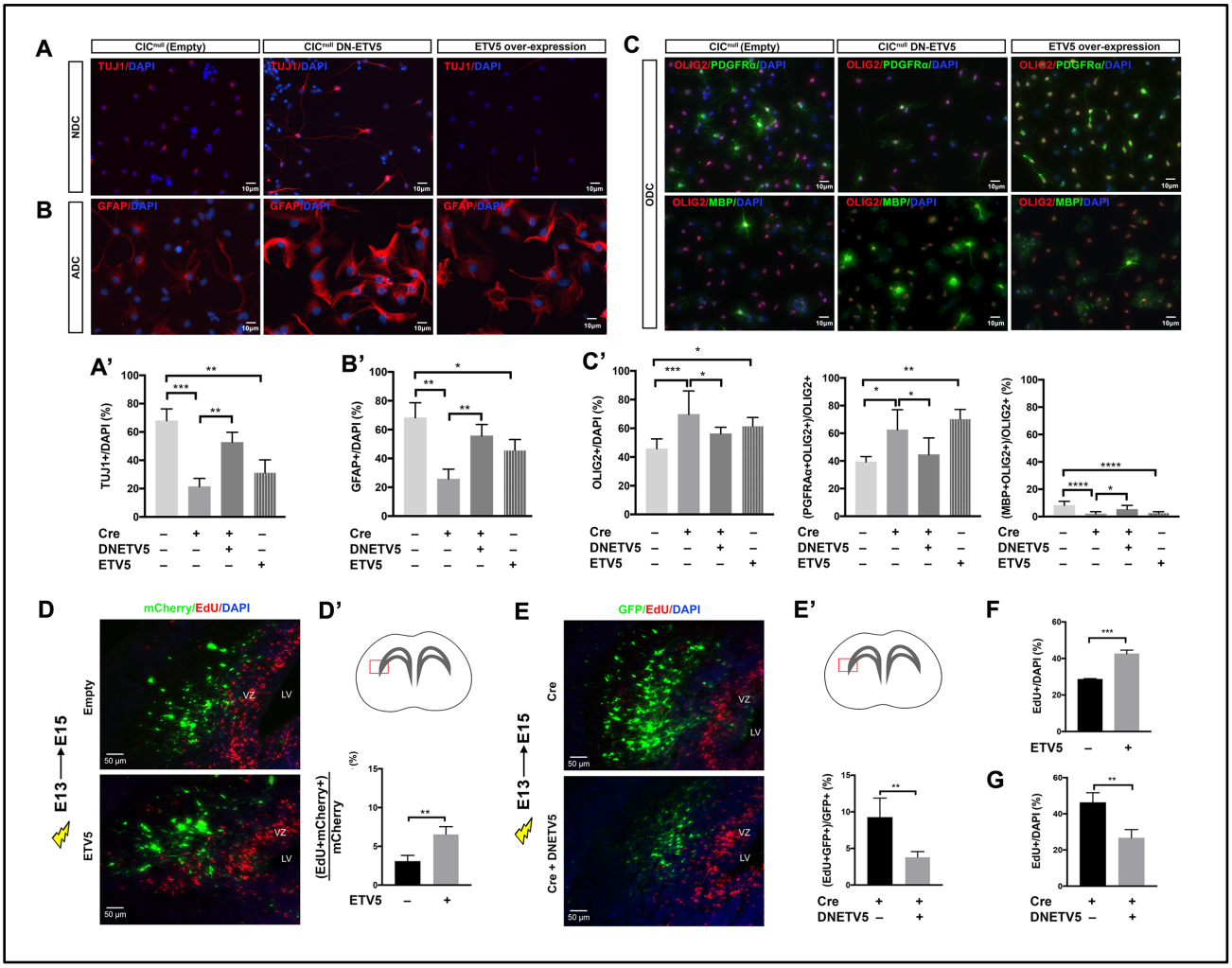

FIGURE 8: Etv5 is necessary and sufficient for proliferation and cell fate bias effects downstream of Cic loss. Cic-null cells with and without DN-ETV5, and Cic-wildtype cells with Etv5 overexpression were assessed for their ability to differentiate in response to 10-days' exposure to lineage-directed differentiating conditions. (A,A') Neuronal differentiation capacity was assessed by bIII-Tubulin immunostaining (Tuj1 positivity), (B,B') astrocytic differentiation capacity was assessed by Gfap immunostaining, and (C,C') oligodendroglial differentiation capacity was assess by staining for Olig2, Pdgfra, and Mbp. (D,D') EdU incorporation 2 days post-electroporation of wildtype *ETV5* or empty control plasmid, both carrying mCherry as a marker, into E13 CIC$^{Fl/Fl}$ VZ. Note: mCherry fluorescence and EdU staining were false-colorized to green and red after grayscale imaging. (E,E') EdU incorporation 2 days post-electroporation of Cre only or of Cre co-electroporated with *DN-ETV5* into E13 CIC$^{Fl/Fl}$ VZ . EdU incorporation assay in cultured NSCs showing (F) effects of ETV5 overexpression in CIC-wildtype NSCs and (G) effects of *DN-ETV5* expression in Cic-null NSCs. Data shown as mean ± SD from n ≥ 4 mice per each group for in vivo studies and n=3 biological replicates for cell culture studies. Statistical analyses performed either t-test in D', E', F, G; or with ANOVA with Tukey's posthoc test in A', B', C'. ns-not significant, *p<0.05, **p<0.01, ***p<0.0001. ADC–astrocytic differentiation condition, NDC–neuronal differentiation condition, ODC–oligodendrocytic differentiation condition. VZ–ventricular zone, LV–lateral ventricle.

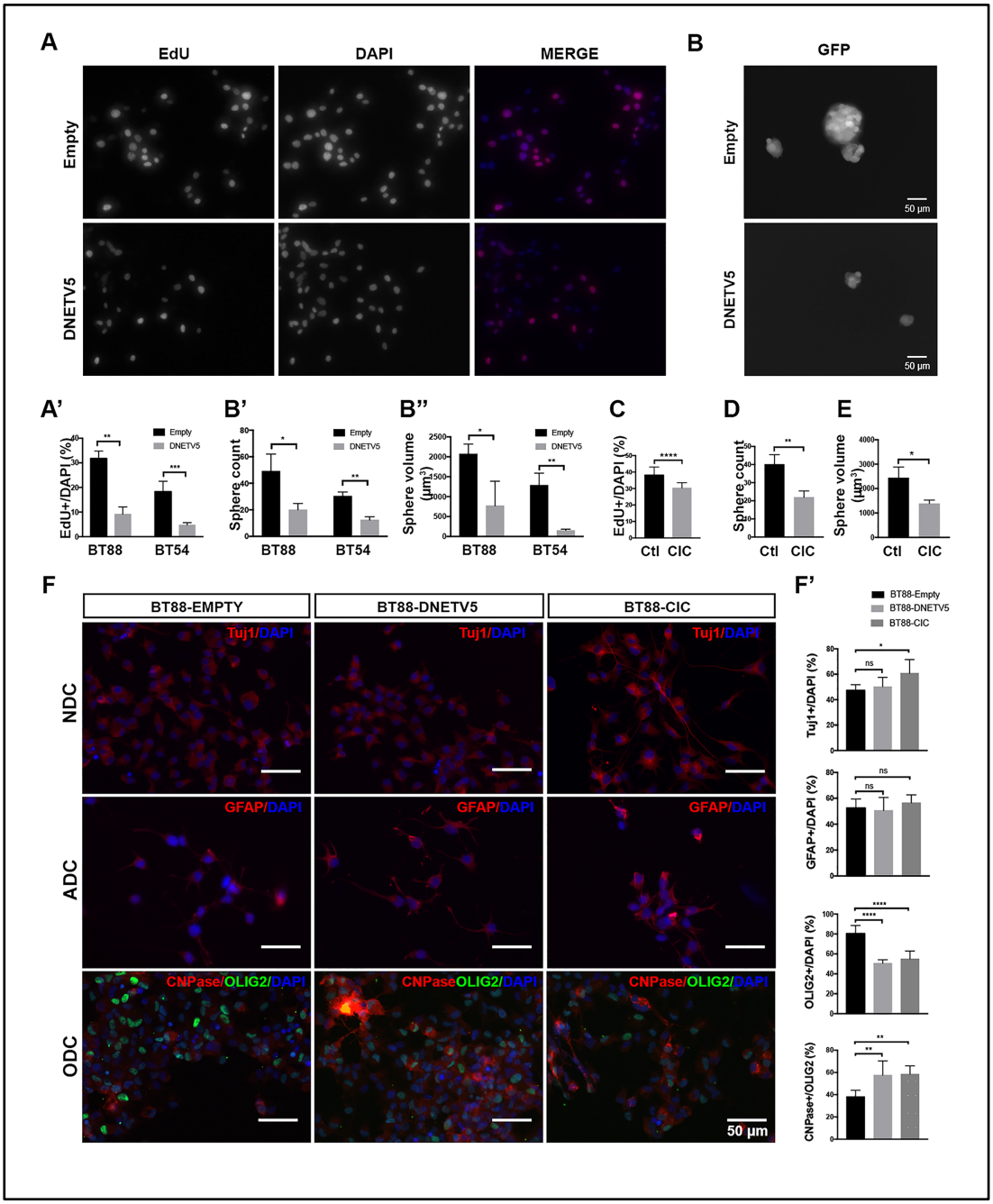

FIGURE 9: ODG cells require CIC loss or elevated ETV5 to maintain proliferation and stemness. (A,A') EdU incorporation in BT-88 and BT-54 ODG cell lines stably transfected with control plasmid or of DNETV5. Quantitation shows results from both cell lines. Representative images are from BT-88. (B) Representative images showing effect of DN-ETV5 on sphere formation in BT88 ODG cells. Quantification of (B') sphere number and (B") size in BT-54 and BT-88 ODG cells without and with DNETV5. (C,D,E) CIC re-expression in BT-88 cells decreases proliferation, sphere number, and sphere size. (F,F') Lineage-specific differentiation capacity of BT-88 ODG cells stably transfected with either control plasmid, DNETV5, or CIC; expression of Tuj1, GFAP, OLIG2, and CNPase after 10-days exposure to differentiation conditions for neurons, astrocytes, and oligodendrocytes. Data shown as mean ± SD from n=3 biologic replicates. Statistical analyses by ANOVA with Tukey's posthoc test. ns-not significant, *p<0.05, **p<0.01, ****p<0.0001. NDC–neuronal differentiation condition, ADC–astrocytic differentiation condition, ODC–oligodendrocytic differentiation condition.

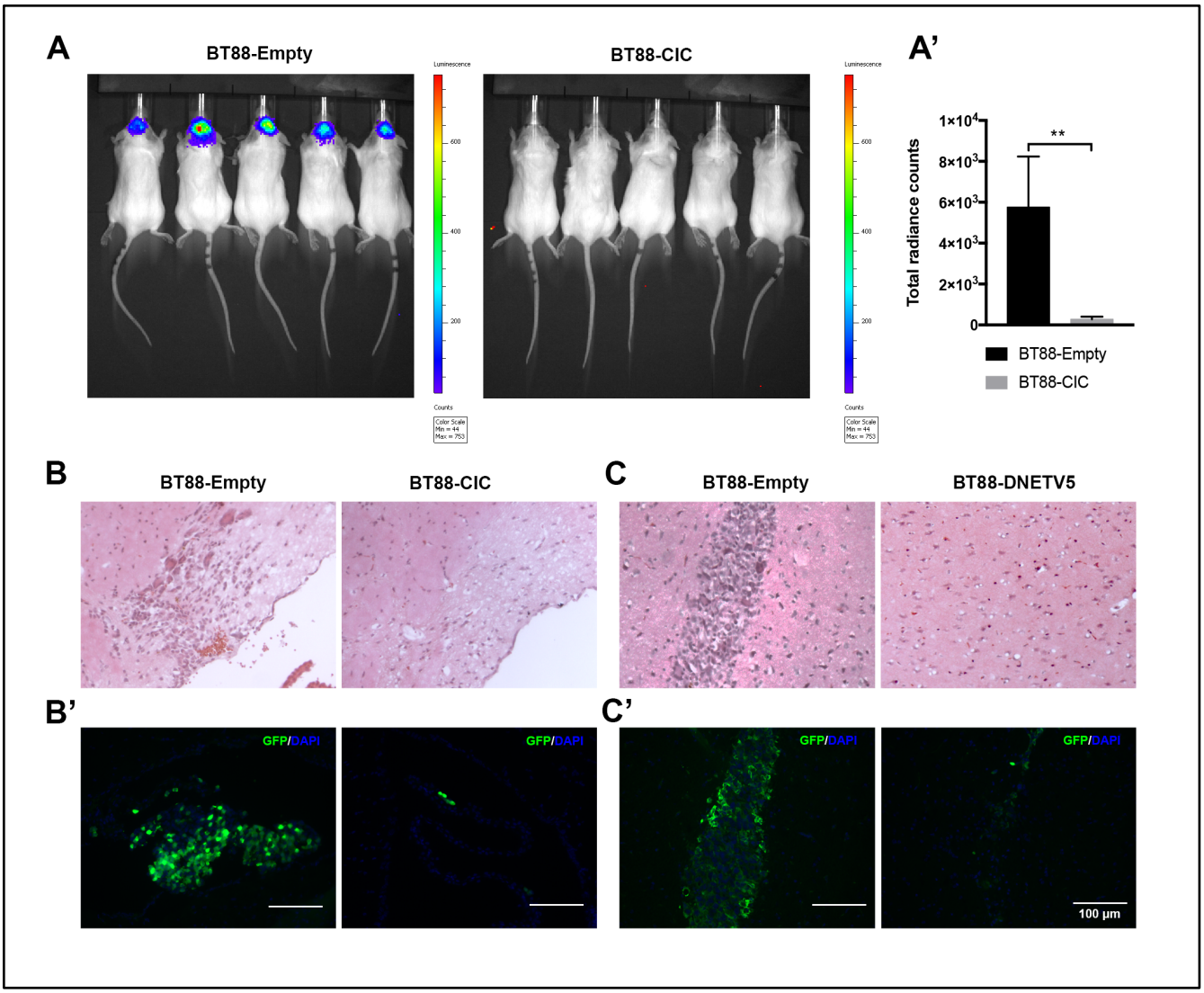

FIGURE 10: Tumorigenicity of ODG cells is reduced by CIC re-expression or ETV5 blockade. (A, A') Bioluminescence imaging of NOD-SCID mice at 6 weeks post-implantation of BT88 oligodendroglioma cells stably transfected with either empty-GFP-luciferase or CIC-GFP-luciferase expression vectors. (B,B') Representative images of brain sections from mice implanted with control-GFP-luciferase BT88 cells or CIC-GFP-luciferase BT88 cells stained with H&E or GFP. (C,C') Representative images of brain sections from mice implanted with control-GFP BT88 cells or DNETV5-GFP expressing BT88 cells stained with H&E or GFP. Data shown as mean ± SD from 8 mice per group. Statistical analyses by student's t test. **$p<0.01$.